Development of Bi-layer Engineered Cardiac Tissues Containing Cardiomyocytes and Microvessels

A DISSERTATION
SUBMITTED TO THE FACULTY OF
UNIVERSITY OF MINNESOTA
BY

Jeremy Adam Schaefer

IN PARTIAL FULFILLMENT OF THE REQUIREMENTS
FOR THE DEGREE OF
DOCTOR OF PHILOSOPHY

Robert T. Tranquillo, Adviser

August 2016

Acknowledgements

I am incredibly grateful to everyone that has helped me on this long, challenging, and ultimately rewarding journey. First and foremost, I would like to thank my mother, Judy, for her love and support. She has always encouraged me and offered her guidance and a boost to my confidence when I've needed it most. Without her, this work would never have been attempted, let alone completed.

I would like to express my gratitude to my adviser, Bob Tranquillo, for his guidance and support. Thank you for providing me with this incredible opportunity to work on such a cutting-edge project. I appreciate your mentorship over the last five years, and will use the skills you have helped me develop throughout my career.

I did not complete this work on my own, and I owe a great deal to current and former lab members. Thank you to all those who took the time to teach me new skills upon my arrival. I owe special thanks to Sonja Riemenshneider, Jackie Wendel, and Zach Galliger, my companions on the heart patch project for teaching me everything about microvessel patches and animal studies, as well as for cherished friendship. Thank you to Susan Saunders for all of her assistance with the animal study in this work. Your skill on the cryostat and histology bench helped more than you can know. Thanks to Jill Schmidt and Jay Reimer, fellow Tranquillo West lab members, for your friendship and general help around lab. I'd also like to thank Jackson Baril for all of his hard work and evenings and weekends spent in lab. Finally, I'd like to thank Zeeshan Syedain, Sandy Johnson, and Naomi Furgeson for their help troubleshooting problems and keeping the lab running smoothly.

I would also like to thank my funding sources during my time in graduate school. Without this financial support, the work documented here would never have been possible. Thank you to Victor Barocas, Patrick Alford, and Angela Panoskaltsis-Mortari for providing me with a project and funding the summer before starting graduate school. Thank you to St. Jude Medical, who provided a fellowship for my first semester of studies. Finally, thank you to the National Institutes of Health for the R01 that funded the majority of this work.

I would like to thank my fellow graduate students who have become my close friends. I will always remember our large group lunches, theme parties, and happy hours fondly. The daily discussions from the lighthearted to the serious were important in maintaining sanity along the way. Your support and advice, so freely and honestly given, is a testament to how wonderful you all are.

Last, but certainly not least, I would like to thank the rest of my friends and family for their support and confidence in me. Thank you especially to my grandmother, Doris, for being such a warm and positive person throughout my life. You always know how to brighten my spirits when I need it. And to my girlfriend, Antonia, I cannot thank you enough for all that you do for me on a daily basis. Thank you for reading this dissertation and all the offers of help along the way. Most importantly, thank you for being my steadfast support and your unwavering confidence in me.

Dedication

This dissertation is dedicated to my friends and family who have supported me through this long journey. I would not have completed it without you.

I would also like to dedicate this to Mr. James Jerome, one of the best teachers I've ever had. Your Biology 2 class started me down the path to becoming a Biomedical Engineer. Thank you.

Abstract

The prevalence of coronary heart disease and myocardial infarction coupled with the limited availability of donor hearts to replace damaged tissue leaves many patients with insufficient treatment. Cardiac tissue engineering has emerged to attempt to fill this need, but engineered cardiac tissues are limited in size by a lack of vascularization. In this work, we aim to create a vascularized cardiac tissue through the combination of an established microvessel construct with a cardiomyocyte construct, and we investigate its use in a nude rat model of myocardial infarction. The results detailed in this dissertation indicate that the bi-layer construct not only improves contractile function of the cardiomyocytes, but also that the human microvessels can sprout into the cardiomyocyte layer and become perfused when implanted *in vivo*.

Table of Contents

List of Tables

List of Figures

Chapter 1. Introduction

1.1 Background

Coronary heart disease (CHD) accounts for nearly 1 in 7 deaths each year in the United States[1]. CHD often progresses to myocardial infarction (MI) when occlusion of one of the coronary arteries prevents blood from reaching the myocardium and results in cell death. Depending on the severity of the MI, up to one-quarter of the total cells in the heart may die [2]. Unfortunately, the heart has a very limited ability to replace the cardiomyocytes that are lost, and a fibrotic scar ultimately forms in the infarction area. This scar formation is accompanied by other deleterious changes to the heart, including ventricle dilation and thinning of the ventricular wall. Current post-infarction treatments are also incapable of repairing this cellular damage once it has occurred and are mainly limited to preventing further damage and treating symptoms of the disease. The only true method to replace the damaged myocardium is whole organ transplantation.

Due to the shortage of available donor hearts and the prevalence of CHD, other treatments are being investigated. Pioneering studies have utilized cells injected into the damaged myocardium of patients after MI. Different cell sources have been used for these treatments including bone marrow derived stem cells[3, 4] and skeletal myoblasts [5, 6]. These studies have shown some benefit to minimizing ventricular wall thinning and improving ejection fraction. However, investigations of cell retention in animal models have shown many cells are not retained in the area of interest[7]. Cardiac tissue engineering seeks to produce engineered cardiac tissues (ECTs), tissues containing

cardiomyocytes, *in vitro* that can deliver and maintain large numbers of cells and replace or augment damaged tissue after myocardial infarction.

One of the critical remaining obstacles to the generation of physiologically relevant ECTs is vascularization of the tissue. The high metabolic demand of native myocardium requires a dense microvessel network of approximately 2,000 capillaries per square millimeter, or a spacing of only 20 µm between capillaries [8]. However, neither ECTs nor engineered microvessel tissues have been able to produce densities higher than 940 capillaries/mm^2 [9]. Despite promising results of ECTs at ameliorating deleterious remodeling of the myocardium, microvessel incorporation is a necessity before clinical relevance can be achieved.

This chapter will provide an overview of the current approaches for the generation of ECTs and microvessel tissues *in vitro*. Discussion will cover common cell choices and fabrication techniques, *in vitro* conditioning, and strategies to connect ECTs with microvessel networks.

1.2 Cell selection

1.2.1 Cells for creation of engineered cardiac tissues

1.2.1.1 Neonatal rat cardiomyocytes

Initially, studies in the field of cardiac tissue engineering were carried out using primary cells isolated from neonatal rat hearts. These cells have since seen extensive use for the construction of ECTs [10-14], and are well characterized. Large numbers of such cells can be easily isolated, resulting in their continued use in the development of new systems. Despite this utility, ECTs made from non-human cell sources will never be fit

for clinical use and a source for large numbers of human cardiomyocytes is therefore required.

1.2.1.2 Embryonic stem cell derived cardiomyocytes

Creation of human embryonic stem cells (ESCs) [15] provided a source of easily expandable pluripotent cells, those with the potential to differentiate into any type of cell found in the body. Mouse ESCs had previously shown the capacity to generate cardiomyocytes through the use of embryoid bodies [16], and this was also the first method to produce functional cardiomyocytes using human ESCs [17]. Differentiation protocols have advanced to methods that leverage signaling pathways from developmental biology to make this process more efficient [18]. However, because the creation of ESCs requires the destruction of a viable human embryo, use of human ESCs carries ethical baggage that has limited their acceptance.

1.2.1.3 Induced pluripotent stem cell derived cardiomyocytes

In 2007, human induced pluripotent stem cells (hiPSCs) were created by reprogramming adult cells using four transcriptions factors: Oct4, NANOG, LIN28, and SOX2 [19, 20]. This breakthrough opened the door for autologous sources of pluripotent stem cells, and also eliminated the ethical concerns associated with the use of ESCs. Differentiation of hiPSCs into cardiomyocytes was demonstrated shortly after [21]. hiPSC derived cardiomyocytes (hiPSC-CMs) have also been generated from patients with congenital defects to facilitate study of these diseases [22, 23]. hiPSC-CMs obtained from the laboratory of Dr. Timothy Kamp at the University of Wisconsin were used in this

dissertation for their potential to be autologously sourced and have a demonstrated potential for ECT construction [24, 25].

1.2.1.4 Non-cardiomyocytes

Engineered cardiac tissues are never made solely with cardiomyocytes. Each of the three sources described above utilize a mixed population of cells containing cardiomyocytes and non-myocytes. The isolation of neonatal rat cardiomyocytes involves digestion of whole hearts, and results in a CM fraction of only 40-50%, with the rest being composed of fibroblasts, smooth muscle cells, endothelial cells [26]. Even the most efficient differentiation protocols for ESCs and hiPSCs only produces CM yields of 60-90% [18]. The remaining fraction is poorly characterized, but is believed to be fibroblast-like.

The non-myocytes in ECTs are actually beneficial to overall tissue function. In tissues made from hydrogels, such as collagen or fibrin, these non-myocytes are required for cell-induced compaction as the cardiomyocytes do not compact the gel. Furthermore, it has been shown that ECTs produce more force with increasing non-myocyte fraction [27].

1.2.2 Cells for engineered microvessel tissues

1.2.2.1 Endothelial cells

A variety of human endothelial cell (EC) sources are available for engineering microvessel tissues. Human umbilical vein endothelial cells (HUVECs) are one of the most common choices [28-30]. While these cells are not autologous, they are well-defined and easily-obtainable. A number of autologous sources of endothelial cells do exist,

including ECs from hiPSCs [31], adipose derived stem cells [32], and blood outgrowth endothelial cells (BOECs) [33]. Of these, BOECs obtained from collaborator Dr. Robert Hebbel at the University of Minnesota were used in this work because they can be autologously sourced, are easily expandable *in vitro*, and exhibit a phenotype characterized by endothelial cell markers (VE-cadherin, flk-1, vWF, CD36), and lack monocyte markers (CD13 and CD45) [33].

1.2.2.2 Support cells

In the native environment, capillaries are closely associated with pericytes (PCs). PCs stabilize capillaries through the secretion of growth factors and ECM remodeling [34]. Their close relationship with capillary ECs also leads to maturation and maintenance of the microvessel network [35, 36]. Other cell types have also been used *in vitro* to fill the support cell role, including mesenchymal stem cells [28, 37] and fibroblasts [38, 39]. Pericytes, obtained from the collaborating lab of Dr. George Davis at the University of Missouri [40], were used in the present body work. In the future, pericytes may be autologously source from skin [41].

1.3 Engineered cardiac tissue and microvessel tissue construction techniques

1.3.1 Seeding of prefabricated scaffolds

Engineered cardiac tissues can be made relatively easily by seeding cells on the surface of a 3D scaffold and many materials have been successfully used for such scaffolds. Synthetic materials such as polycaprolactone (PCL) [42], poly(glycerol-sebacate) (PGS) [43], and poly(lactide-co-glycolide) (PLGA) [44] all allow fine tuning of the

scaffold properties prior to seeding with cells. Natural polymers such as collagen I [45], alginate [46], and gelatin [47] have also been used with prefabrication techniques.

Creation of scaffolds in advance permits the use of fabrication methods that would not be compatible with cells, but allows for fine control over scaffold design. Electrospinning can be used to make small diameter fibers on the order of native extracellular matrix (ECM) fibers in a highly aligned manner that is similar to organization of native tissue [48]. Microfabrication techniques have been used to make scaffolds with precisely defined features that interlock together allowing for easy assembly of larger tissues [49]. Individual units can be seeded with different types of cells and assembled in specific patterns to achieve desired cell distributions and functionalities.

1.3.2 Entrapment of cells in a forming scaffold

Engineered tissues can be formed by suspending cells in a solution, such as collagen I [13, 50] or fibrin [10, 12, 25], that will gel into a 3D scaffold. These tissues are formed by adding the gel-forming solution to a mold, and as the gel begins to set, fibers are formed around the cells, entrapping them evenly throughout. This method does not allow for highly aligned matrix fibers to be formed from the outset, and relies on cell-induced gel compaction for any alignment that occurs. However, by thoughtfully designing the mold in which these tissues are formed, strong cell-induced alignment can be achieved as the tissue matures [10].

1.3.3 Non-scaffold based methods

Engineered cardiac tissues have been made without the use of a 3D scaffold through the use of cell sheets [14, 51-53] and layer-by-layer coating of cells [54]. Cell sheets

are formed through the use of a temperature-sensitive substrate. Cells are plated on the substrate, where they deposit their own ECM. The cell sheets are removed by reducing the temperature of the system. By harvesting multiple sheets and layering them on top of one another, thicker ECTs can be formed. This method has also been used with co-culture of endothelial cells to induce vascularization *in vitro* [14]. The layer-by-layer technique utilizes singularized cells that have been coated with layers of ECM nanofilms [54-56]. The cells are then added to a culture dish where the nanofilm coating helps to form cell-cell junctions via integrins. By adding endothelial cells, capillaries could be introduced into these tissues as well [54].

1.4 *In vitro* conditioning techniques for engineered cardiac tissues and microvessel tissues

A major advantage in the creation of ECTs is the ability to condition these tissues *in vitro* prior to implantation. Conditioning regimens can help to improve tissue function, cell survival, and mechanical properties of the tissue itself.

1.4.1 Mechanical loading

During the cardiac cycle, cardiomyocytes are exposed to cyclic mechanical stretching. Systems have been implemented to incorporate this important mechanical stimulus to ECTs *in vitro* with positive results. A uniaxial stretch device actuated by electromagnetic force was shown to produce a more mature phenotype in ESC-CMs seeded on gelatin sponges as evidenced by improved cell elongation, ion channel expression, and contractile protein expression [57]. Previous work from our laboratory has demonstrated that cyclic mechanical stretch applied to a ring-shaped ECT mounted on

pneumatically distended latex tube resulted in a two-fold increase in twitch force production [12].

1.4.2 Electrical stimulation

Cardiomyocytes are an electrically active cell type, and their contraction is controlled by electrical signals in the heart's sinoatrial node. However, when grown on 2D culture plastic or 3D ECTs, CMs beat spontaneously. Because there is no neural control, these contractions are dyssynchronous and irregular contractions of the tissue. Studies have shown that external electrical stimulation during culture has positive effects on the ECTs. Primary functional improvements include increase in contractile force and calcium handling due to improved sarcomere organization and improved connexin-43 expression [58]. Cardiac-specific genes have been shown to increase in expression indicating CMs can be matured through the use of electrical stimulation as well [59].

1.4.3 Perfusion

Because of the high metabolic demand of cardiomyocytes, the size of ECTs is limited by the need for nutrients and oxygen to diffuse from the surrounding culture medium. By perfusing medium through a porous scaffold, larger tissues can be made. This method has been shown to improve cell viability in multiple studies [11, 60, 61]. These studies also showed improvement in electrical properties [11, 61] and sarcomeric organization [60].

Perfusion systems have been used with microvessel tissues both in microfluidic systems [30, 62, 63] and in larger engineered tissues [9]. Microfluidic systems have demonstrated that interstitial flow facilitates the sprouting of microvessels from

endothelialized perfusion channels [64, 65]. Low levels of interstitial flow through a fibrin tissue was shown to increase total cross-sectional lumen density and confer barrier function to the microvessels [9].

1.5 Vascularization of engineered cardiac tissue strategies

Vascularization of ECTs is a necessity before they can be used in a clinical setting. Different techniques have been utilized to induce vascularization in ECTs, yet none have produced vessel densities approaching that of the native myocardium. Cardiomyocytes mixed with endothelial and support cells have been cast into bulk collagen gels [24] as well as seeded onto preformed poly-1-lactic acid/polylactic glycolic acid (PLLA/PLGA) scaffolds [44, 66]. While vessel-like structures were found *in vitro*, the number of lumen structures were less than 15 per square millimeter [24, 44]. Upon implantation onto normal rat hearts, implanted vessels became functionally integrated with the host vasculature [24, 66]. Cell sheet technology has been used to induce vascularization by co-culture of neonatal rat CMs with ECs in the same sheet [14]. The endothelial cells in the sheet form a microvascular network prior to layering three sheets together. When implanted onto an infarcted rat heart, the layered co-culture cell sheets improved cardiac function and contained a higher capillary density compared to cell sheets without ECs [14].

1.6 Current deficiencies and obstacles

Although progress has been made in cardiac tissue engineering towards the generation of functional myocardium, significant shortcomings remain. Foremost is the size of the tissues. As outlined above, ECTs of a clinically relevant size cannot currently

be developed due to a lack of vascularization. Without a vascular network to deliver oxygen and nutrients deep within the tissue, diffusion alone must support cellular metabolic demands *in vitro*. When implanted into an animal, unvascularized tissues must wait for angiogenesis, during which time cell death may occur. While co-culture with vascular cells has resulted in ECTs containing microvessels, their density is orders of magnitude short of native myocardium. The state-of-the art stem cell-derived CMs now seeing increased use have shown great promise for their potential to generate patient-specific cells, as well as their use for disease model cells. Their differentiation products, however, are not a well-defined population. The resultant non-myocytes have not been extensively characterized, and the CMs are a mix of atrial, pacemaker, and ventricular cells. The CMs also exhibit an immature phenotype, with different functional properties than adult myocytes. Which maturation state is most desirable for cardiac repair is still unknown.

Chapter 2. Tissue Contraction Force Microscopy for Optimization of Engineered Cardiac Tissue

The material discussed in this chapter is adapted from the following:

Schaefer, J.A., et al. Tissue Contraction Force Microscopy for Optimization of Engineered Cardiac Tissue. Tissue Engineering: Part C. 2016.[67]

2.1 Abstract

We developed a high throughput screening assay that allows for relative comparison of the twitch force of millimeter-scale gel-based cardiac tissues. This assay is based on principles taken from traction force microscopy and utilizes fluorescent microspheres embedded in a soft polydimethylsiloxane (PDMS) substrate. A gel-forming cell suspension is simply pipetted on to the PDMS to form hemispherical cardiac tissue samples. Recordings of the fluorescent bead movement during tissue pacing are used to determine the maximum distance that the tissue can displace the elastic PDMS substrate. In this study, fibrin gel hemispheres containing hiPSC-derived cardiomyocytes (hiPSC-CMs) were formed on the PDMS and allowed to culture for nine days. Bead displacement values were measured and compared to direct force measurements to validate the utility of the system. The amplitude of bead displacement correlated with direct force measurements and the twitch force generated by the tissues was the same in 2 and 4 mg/ml fibrin gels even though the 2 mg/ml samples visually appear more contractile if the assessment were made on free floating samples. These results demonstrate the usefulness of this assay as a screening tool that allows for rapid sample preparation, data collection, and analysis in a simple and cost effective platform.

2.2 Introduction

Engineered cardiac tissues (ECTs) can be a useful tool when investigating novel drug treatments and, potentially, for the replacement or augmentation of damaged tissue *in vivo*. With the discovery of human induced pluripotent stem cells[19] (hiPSCs) and the development of fast and efficient differentiation protocols to generate cardiomyocytes[18], researchers have the ability to utilize both healthy and pathological cardiomyocytes[22, 23, 68] to generate engineered tissues. However, many factors such as cellular density, gel scaffold composition, growth medium, medium supplements, and experimental drugs need to be assessed experimentally for their effect on cell and tissue function in order to generate physiologically relevant *in vitro* tissue models.

Cell traction and contraction are fundamental cell behaviors that require quantification during design, development, and characterization of many engineered tissues. The cell types predominantly responsible for these forces are interstitial cells, most notably fibroblasts, and muscle cells, such as cardiomyocytes and skeletal myoblasts. Interstitial cell types entrapped in a fibrillar network such as collagen or fibrin exert cell traction forces that are responsible for compaction of the bulk gel, which can result in desired matrix fiber and cell alignment[69, 70]. Similarly, cardiomyocytes and skeletal myoblasts generate considerable contractile forces as their primary function, which can be visualized with a microscope in small tissues or unaided in larger tissues. It is desirable for engineered muscle tissues to be able to reproduce these forces. As a result, many systems have been developed to measure traction forces or contraction forces of single cells or 3D tissues.

Single-cell level assays such as traction force microscopy[71] or microfabricated posts[72, 73] have been used to determine forces exerted by single cells including cellular responses due to soluble factors[74] and substrate stiffness[75-77]. However, these assays do not capture the complex 3D environment that cells experience *in vivo* or in an engineered tissue construct. Not only do extracellular matrix properties regulate cellular function[78], cell-cell interactions are important determinants of tissue properties as well. For example, both skeletal myoblasts and cardiomyocytes in mature muscle exist in a syncytium that aids in the rapid conduction of electrical signals necessary for coordinated contraction. Most tissues also have characteristic alignment that may not be captured by assays of single cells on a 2D substratum.

Tissue level assays have also been developed and include free-floating tissue samples, as well as anchored tissues of both macro and micro scale that have proven useful for investigating the role of alignment[10], matrix stiffness[79], and matrix composition[80]. However, free-floating assays do not measure cell forces directly, instead rely on theory to relate the tissue compaction to cell forces[81, 82]. And while macro sized tissues[10] are easy to prepare and conducive to force measurement without highly specialized equipment, they are low-throughput and screening many factors quickly becomes cumbersome and taxing on resources. Conversely, micro sized tissues enable high-throughput screening, but generally require microfabrication[79, 83] or the use of specialized equipment[84].

Herein we propose and validate a new approach, which we term tissue contraction force microscopy, inspired by cell traction force microscopy that combines simplicity of sample preparation and the use of common lab equipment. Rather than measure fluorescent microsphere displacements due to forces exerted by single cells on

a polydimethylsiloxane (PDMS) or polyacrylamide (PA) membrane, we measure microsphere displacements due to forces collectively exerted by cells in 50 µl tissues formed by simply pipetting the gel forming cell suspension directly onto the surface of a PDMS membrane, resulting in hemispherical-shaped tissue constructs. Since fibrin gel is a common choice for ECTs[10, 27, 85], to demonstrate the utility of this approach, we compared microsphere displacements generated by ECTs fabricated from hiPSC-CMs in fibrin gels at two different fibrin concentrations as well as two different cell concentrations and then directly measured the forces in the same samples as a validation of the assay. These ECTs were also characterized histologically to provide insight as to how gel compaction might affect the measured bead displacements.

2.3 Materials and Methods

2.3.1 Culture dish preparation and characterization

To form the PDMS substrate, 1 ml ($4.55x10^{10}$ particles/ml) of 1 µm diameter yellow-green fluorescent microspheres (Polysciences, Inc.) were desiccated overnight under vacuum. Drying is necessary because the microspheres are suspended in water which does not mix well with the hydrophobic PDMS and results in an unusable substrate. Once dried, the beads were dissociated into a fine powder using a mortar and pestle and mixed with 40 grams of Slygaard 527 PDMS (Ellsworth Adhesives) at a 1:1 mixing ratio (Part A:Part B). The PDMS components and microspheres were mixed by hand for 5 minutes before being centrifuged at 1000g for 10 minutes to remove clumps. The supernatant, containing primarily singularized microspheres, was decanted into a plastic cup, and the PDMS-microsphere mixture was poured into 35 mm Petri dishes (BD Falcon). To maintain uniform thickness between dishes, 1 gram of the PDMS

mixture was added to each dish before being placed into a 90° C oven overnight. Dishes are stored with the lids on to prevent accumulation of dust and debris on the PDMS surface before sterilization. Immediately prior to use, the cured dishes were sterilized with a UVO cleaner (Model 342A; Jalight Company, Inc.) for 4 minutes with the lids off and then transferred to a sterile culture hood.

Uniaxial strain to failure testing was conducted on three substrate samples from three separate batches of PDMS-microsphere mixture. A 2 cm x 1 cm rectangular sample was removed from the Petri dish using a flat cell scraper (BD Falcon). Thickness of the samples was measured using a digital caliper. Samples were mounted into grips attached to the tester's actuating arms, preloaded to 0.005 N, and then strained to failure at 3 mm/min using an Instron MicroBionix (Instron Systems). Strain was calculated by taking the natural logarithm of the sample's deformed length over the initial length, and stress was defined as the force divided by the undeformed, cross-sectional area of the sample. Young's modulus was taken as the slope of the linear region of the stress-strain curve.

2.3.2 Cell and ECT culture

Human iPSC-derived cardiomyocytes were obtained from the lab of Dr. Timothy Kamp at the University of Wisconsin-Madison. Cells were differentiated via the small molecule Wnt/GSK3 inhibition (GiWi) protocol[18] from hiPS cell line DF19-9-11T. The purity of the differentiated cells was determined by flow cytometry for cardiac troponin-T (cTnT)+ cells at day 15 of differentiation to be 75-95% cTnT+. Cells were frozen in 90% FBS and 10% DMSO at $10x10^6$ cells/vial and stored in liquid nitrogen before shipping. hiPSC-CMs were thawed into 2 $\mu g/cm^2$ fibronectin-coated (Sigma) T75 flasks and

cultured in 15 ml EB-20 medium (DMEM/F12 basal medium (Corning), 0.1 mM 2-mercaptoethanol (Sigma), 0.1 mM nonessential amino acids (Hyclone), 1 % penicillin/streptomycin (Gibco), and 20% FBS). Medium was replaced 24 hours after thaw to remove any residual DMSO and dead cells and changed to 2% FBS medium (EB-2) 48 hours post thaw. Cells were kept in culture until they resumed beating (approximately 4-7 days) before harvesting with 0.25% Trypsin/EDTA (Hyclone) + 2% chicken serum (Sigma). Trypsinized hiPSC-CMs were added to a mixture of Medium 199 basal medium (M199, Life Sciences) and a fibrin-forming solution, consisting of varying fibrinogen (Sigma) concentrations and thrombin (Sigma) to catalyze gel formation. Final concentrations of the gels comparing fibrinogen concentrations were either 2 or 4 mg/ml fibrinogen, 1.25 U/ml thrombin, and 4 million hiPSC-CMs/ml. For cell concentration experiments, final concentrations of gels were 4 mg/ml fibrinogen, 1.25 U/ml thrombin, and either 3 or 5 million hiPSC-CMs/ml. Immediately after mixing, 50 µl hemisphere gels were cast as droplets directly on the surface of prepared PDMS coated dishes in a single line through the center of the dish. Gels were incubated for 4 minutes at room temperature in the sterile culture hood before being moved to 37° C, 5% CO_2 incubator for a further 10 minutes to complete polymerization, after which 2.5 ml EB-20 medium supplemented with 2 mg/ml ε-aminocaproic acid (ACA, Acros Organics) was added to the dishes to completely cover the hemispheres. Medium was changed 24 hours after casting, and switched to EB-2 + ACA after 48 hours. Constructs were cultured for a total of 9 days with media changes every other day before analysis of beating.

2.3.3 Microsphere displacement measurements

Displacement of fluorescent microspheres were captured on an Olympus IX81 inverted microscope with heated environmental chamber (Precision Plastics) at 37° C using Metamorph 7.7.8.0 (Molecular Devices Inc.). Prior to testing, medium was supplemented with 2 mM $CaCl_2$. During testing (**Error! Reference source not ound.**A), the constructs were paced via field stimulation (Grass S88X Stimulator; Asto-Med, Inc.) provided by silver wire electrodes and a square wave function of 24 V peak voltage, 10 ms pulse width, and 0.5 Hz frequency. This stimulation regime was chosen to ensure that all of the cells within the ECT were contracting at the same time while allowing for complete relaxation before the next stimulation pulse. Fluorescent image series and a single brightfield image were taken at each of four locations around the perimeter of each construct. The fluorescent image series was composed of 25 images taken using Metamorph's Stream Acquisition function, covering 3-5 seconds of real time, or 1-2 complete contraction cycles. While the movement of the microbeads directly under the tissue could be measured, doing so would likely lead to increased variability and a reduction in the observed displacements. Because the ECT is disk shaped and contracting radially inwards, the microbeads at the tissue edge will have the greatest movement directed inwards towards the center of the ECT. Due to the bottom surface of the PDMS substrate being fixed to the Petri dish, the upper surface that is attached to the ECT moves more than the microspheres deeper in the substrate. Therefore, the recordings of the microsphere movements are limited to the top of the PDMS substrate. This is accomplished by moving the microscope objective above the substrate surface, then slowly moving it downwards until microspheres become resolved.

Microsphere displacement was analyzed using the 2D particle tracking feature of the MosaicSuite plugin[86] for ImageJ (NIH). The plugin features three tunable parameters for particle detection: radius, cutoff, and percentile or absolute setting. The radius is the approximate radius of the microspheres to be tracked as they appear in units of pixels in the images. It is recommended to use a slightly larger radius than what would appear in the images. The default value of 3 was appropriate for the 1 μm microspheres used here. The cut-off score is used to eliminate non-particles, where a higher score detects fewer particles. The default value of 3 was used in this study. The percentile/absolute setting is used to determine which fraction of the bright pixels to use in particle detection. When the percentile mode is used, the value set here indicates that the r-th highest percentile of pixel intensities considered. When the absolute mode is used, the value entered indicates the intensity values above which are considered for tracking. The percentile mode was used here and value changed as needed to increase the number of tracked particles, but 0.35 was used in most cases. There are three standard parameters that can be tuned for linking particles once detected: displacement, link range, and dynamics. Displacement describes the maximum distance in pixels a particle will be linked between two frames of the series. Link range is the number of consecutive frames that are considered when tracking particles. The dynamics setting describes the type of particle motion to consider and includes Brownian, constant velocity, and straight line. These settings introduce penalizations to particle motions that do not fit the prescribed style of motion. The default settings of 10 and 2 were used for displacement and link range, respectively, while the straight line dynamics was used to minimize inappropriate perpendicular particle linking.

After tracking all microspheres in an image series, the results were filtered to only include microspheres that were traced through all 25 images of the series, and only traces within 200 pixels of the tissue edge were quantified (**Error! Reference source ot found.**). Due to the linear elastic nature of the PDMS, microspheres further from the tissue edge exhibit reduced movement and would decrease the calculated mean displacement and increase variability. Analysis of microsphere displacements in 200 pixel bins from the tissue edge revealed an approximate 12% decrease in displacement in each bin after the first. However, because of the high density of microspheres in the substrate, the first 200 pixel bin from the tissue edge still provides sufficient numbers of microspheres for analysis. Tissue edge location was determined using the brightfield image taken during data collection. Microsphere location data was imported into a custom Matlab script that calculates the displacement of each microsphere based on its recorded (x,y) positions in each frame. The displacements calculated at each of the four fields are then used to create an average displacement per tissue construct, yielding three measurements per fibrinogen condition.

2.3.4 System validation by direct twitch force measurement

While the bead-tracking system does not allow for direct measurement of forces produced by constructs, it does allow for comparisons of beat strength relative to one another. This is possible because dishes are coated with the same mass of PDMS-microsphere mixture and experiments are cast using dishes from the same batch of PDMS. In order to verify that the relative comparisons of beat strength are valid, the twitch force produced by our hemispherical constructs was measured on a modified, custom-built force testing system[10] (**Error! Reference source not found.**B). Briefly, the

ystem is composed of a media bath with a fixed post cemented to the bottom as well as two carbon pacing electrodes. A second post is attached to a force transducer and records the generated twitch forces of the paced construct. In order to modify the system, initially designed to test larger tissue engineered rings, 25 gauge needles were attached to the two existing posts using PTFE tape. For these validation tests, microsphere displacement measurements were taken prior to removing the construct from the PDMS coated Petri dish and impaling the compacted hemispherical constructs near their periphery onto the needles. Once in place, the construct was pre-tensioned using an adjustment dial and subjected to field stimulation by two carbon electrodes with the same parameters used during bead displacement measurement. Data was collected using LabVIEW and analyzed using a custom Matlab script. Direct twitch force measurements are reported as force normalized to the number of input cardiomyocytes. This allows for easier comparison of ECTs made from different cell numbers, cardiomyocyte purities, and sizes. This metric has been used previously as a way to report the "efficiency of a cardiac tissue engineering system"[27] by describing how the measured forces are related to the initial state of the ECT.

2.3.5 Histology and Immunohistochemistry

Constructs were fixed in 4% paraformaldehyde for 1 hour at 4° C and either whole mount immunofluorescence stained or frozen in embedding medium and cryosectioned into 9 µm thick sections prior to immunofluorescence staining. Samples were permeabilized with 0.1% Triton-X 100 (Sigma), blocked with 5% Normal Donkey Serum (Jackson Immunoresearch), incubated overnight at 4° C in primary antibody followed by incubation at room temperature in secondary antibody and Hoescht 3332

(Life Technologies) for 1 hour. Sections were mounted in fluorescent mounting medium (Dako) before imaging.

2.3.6 Statistics

Data are presented as means ± standard deviations of n=3 experiments each involving 3 replicates for fibrin concentration dependence and one experiment involving three replicates for cell concentration dependence. All results were calculated in Microsoft Excel using Student's t-tests (fibrin and cell concentration dependence) or one-way ANOVA (PDMS substrate thickness and Young's modulus) with p-values < 0.05 considered significant.

2.4 Results

2.4.1 PDMS Substrate Fabrication

A single 40 g batch of PDMS-microsphere mixture resulted in approximately 30 dishes coated with 1 g of material. Variability in the number of dishes was a result of decanting the singularized microsphere mixture from the pelleted clumps after centrifugation. To determine what variability exists between different PDMS samples, three or four samples from three separate batches were mechanically tested. Once cured, the PDMS layer was measured to be 0.94±0.014 (n=4), 0.91 ± 0.02 (n=3), and 0.77 ± 0.05 (n=3) mm thick with corresponding Young's modulus of 8.47±0.92, 6.93 ± 0.48, and 8.0 ± 0.81 kPa, respectively. Variability between replicates of a given batch was minimal. Statistical analysis revealed a difference in the thickness ($p<0.05$), but not in the Young's modulus ($p=0.09$) between batches. These results highlight the importance of using the same batch when making comparisons. While the Young's

modulus is the same between batches, variable thickness may result in different displacements at the surface due to the bottom of the PDMS being fixed to the Petri dish.

2.4.2 ECT Fabrication

Immediately following creation of the fibrin gel hemisphere, the encapsulated hiPSC-CMs were rounded and non-beating. However, within 1-2 days the cells elongated, resumed beating, and began to compact the gel. Initially, contractions were sporadic and limited to individual cells. With increased time in culture, cells began to beat synchronously in small areas, and eventually whole construct contractions were observed. When formed, the construct was hemispherical in shape and approximately 5 mm in diameter and 3 mm thick at the center. However, cell-induced compaction caused the construct to flatten downwards. Final ECT thickness was estimated using cross-sections and determined to be 293 ± 145 μm and 613 ± 129 μm for the 2 mg/ml and 4 mg/ml groups, respectively ($p=0.02$). Because the bottom surface of the gel was constrained to the PDMS substrate, compaction could not occur radially inwards. This led to transverse isotropy where cells appeared aligned in planes parallel to the PDMS substrate (**Error! Reference source not found.**B,D) but exhibited no alignment in the lane when viewed perpendicular to the substrate (**Error! Reference source not found.**A,C).

2.4.3 Microsphere displacement and direct force measurement

Analysis of microsphere displacements with pacing (24V, 10 ms pulse duration, 0.5 Hz) revealed no difference between the 2 mg/ml and 4 mg/ml initial fibrinogen

concentration (22.61 ± 4.66 and 17.80 ± 6.62 pixels, respectively; p=0.37) as shown in **Error! Reference source not found.**A. To validate that the microsphere displacement easurements represented the twitch forces produced by the ECTs, we detached the constructs from the PDMS substrate and attached them to a custom built force measurement system. Direct force measurement (**Error! Reference source not ound.**B) also showed no difference between the 2 mg/ml and 4 mg/ml groups (2.82 ± 1.09 nN/input hiPSC-CM and 2.57 ± 0.80 nN/input hiPSC-CM, respectively; p=0.69). When detached from the PDMS substrate, free-floating deformation of 2 mg/ml ECTs was greater than 4 mg/ml.

Microsphere displacement measurements (Figure 2-5A) of cell concentrations revealed an increased displacement for 5 M cells/ml vs. 3 M cells/ml (5.86 ± 0.58 and 18.59 ± 1.51 pixels, respectively; $p<0.05$). Direct force measurements (Figure 2-5B) of these samples also captured the difference between these two conditions (0.32 ± 0.02 nN/input hiPSC-CM for 3 M cells/ml and 3.58 ± 0.15 nN/input hiPSC-CM for 5 M cells/ml; $p<0.05$).

2.5 Discussion

This study demonstrated that fibrin gels with entrapped cells can be formed directly on the surface of a PDMS substrate, and remain attached without coating the surface with ECM proteins or other functional groups. The PDMS constrains the cell-induced compaction of the gel while providing an auxotonic loading, which occurs with contraction against an elastic boundary. This has been shown to improve ECT twitch force production[13]. ECTs formed as hiPSC-CM-containing fibrin gels were able to displace the microsphere-containing PDMS, which allowed for indirect quantification of

the twitch force. While not reported, contraction and relaxation rates can be directly quantified and compared. The substrate stiffness can be easily tuned by changing the ratio of PDMS components, with an increase in the ratio of part A:B resulting in a decrease in PDMS stiffness. This would allow for investigation of how different elastic loading may affect twitch force production. Decreased PDMS stiffness may also allow for the generation of smaller ECTs, further increasing throughput. PDMS 527 can be made as soft as 0.5 kPa[87], which would potentially allow for ECTs ten-fold smaller to be evaluated. Smaller ECTs were not evaluated in this study because validation using the direct force measurement setup would not have been possible.

The novel tissue contraction force microscopy assay described here is best suited for comparison of tissues with similar thickness, as would occur with application of a drug at varying concentrations to ECTs formed with the same fibrin gel composition. Rather than illustrate this simple application of our HTS, we examined the more complex case of samples with different thickness. Cells distributed throughout a thicker construct may contribute less force towards the deformation of the PDMS substrate due to reduced alignment with and increased distance from the surface. In our comparisons of ECTs made from 2 mg/ml versus 4 mg/ml fibrin, deformation of free-floating 2 mg/ml ECTs was greater than 4 mg/ml ECTs. While this observation could lead to the conclusion that the 2 mg/ml group produces greater force, no difference was measured comparing groups using either our HTS assay or direct force measurements despite the latter being twice as thick. This could be because the reduction in alignment and distance from the substrate does not negatively affect microsphere displacement until large thicknesses are reached.

To evaluate how an increased thickness and associated differences in cell distribution and orientation could affect comparisons in thicker samples, a model based on the anisotropic biphasic theory of tissue-equivalent mechanics[69] could be developed. This theory predicts how cell traction forces induce compaction of a gel's fibrillar network, such as collagen or fibrin, and how this compaction leads to cell and fibril reorientation when there is a mechanical constraint, such as adhesion of the hemisphere at its base to the PDMS. By using this theory to model the cell force transmitted from the gel to the PDMS, the effects of gel compaction and resulting thickness on the bead displacement could be determined and the contraction force per cell estimated.

Differential gel compaction can lead to other complications in interpreting the contractile forces of engineered tissues regardless of the method used. Reduced compaction can lead to reduced cell-cell contacts, which are necessary for the formation of gap junctions and important for the fast propagation of electrical signals[88]. Increased distance between cells may decrease the efficacy of paracrine signals from neighboring cells as well. Finally, constrained gel compaction is the primary effector of cell and fiber alignment in 3D engineered tissues, and comparisons between aligned and isotropic ECTs show alignment leads to increased twitch force[10]. All of these factors associated with differential gel thickness can and will play into the contractile force measured for gel-based ECTs by any method[10, 79-84] and need to be considered when interpreting the data.

In summary, we have described a method for screening forces generated by ECTs in a system based on traction force microscopy that we call tissue force microscopy. This method tracks fluorescent microsphere displacements in a PDMS substrate by the contraction of the tissue. The system can be fabricated and analyzed

using common laboratory equipment quickly and easily, while allowing for multiple samples to be made in the same dish. We generated ECTs from two different fibrinogen concentrations as well as two different cell concentrations, measured the microsphere displacements, and then removed the ECTs from the PDMS to directly measure the contraction forces as validation of the assay.

2.6 Acknowledgements

The authors thank Dr. Patrick Alford for the use of fabrication and live cell imaging equipment, and Susan Saunders for technical assistance. This study was funded by National Institutes of Health award R01 HL108670 (R.T.T.).

2.7 Figures

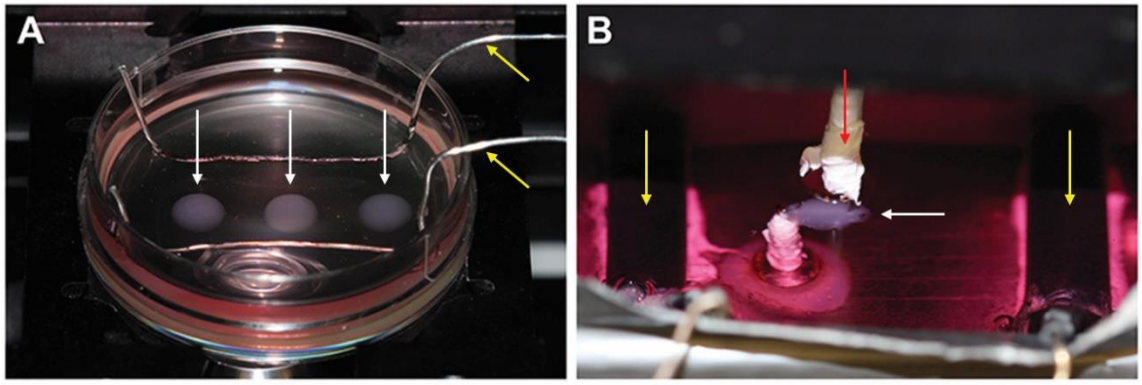

Figure 2-1. Data collection setups

A) Microsphere displacement and **B)** validation force testing setups. Red arrow indicates post attached to the force transducer, yellow arrows indicate pacing electrodes, and white arrows indicate the ECT.

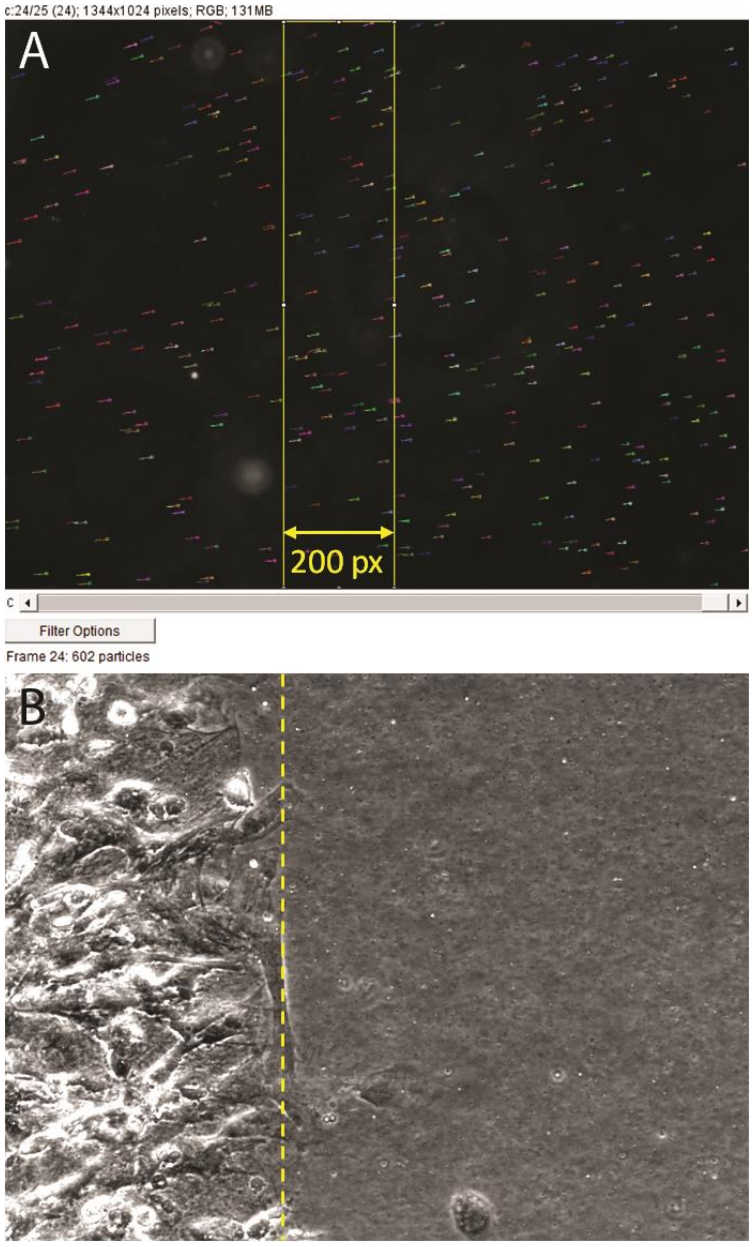

Figure 2-2. Screen captures of microsphere tracing plugin

A) Overlay of traced microsphere trajectories (short multicolored horizontal lines) on a single frame from the series. **B) B**rightfield image used to determine the ECT edge (dashed yellow line). Yellow rectangle in **A)** is the boxed selection of microsphere traces saved for quantification.

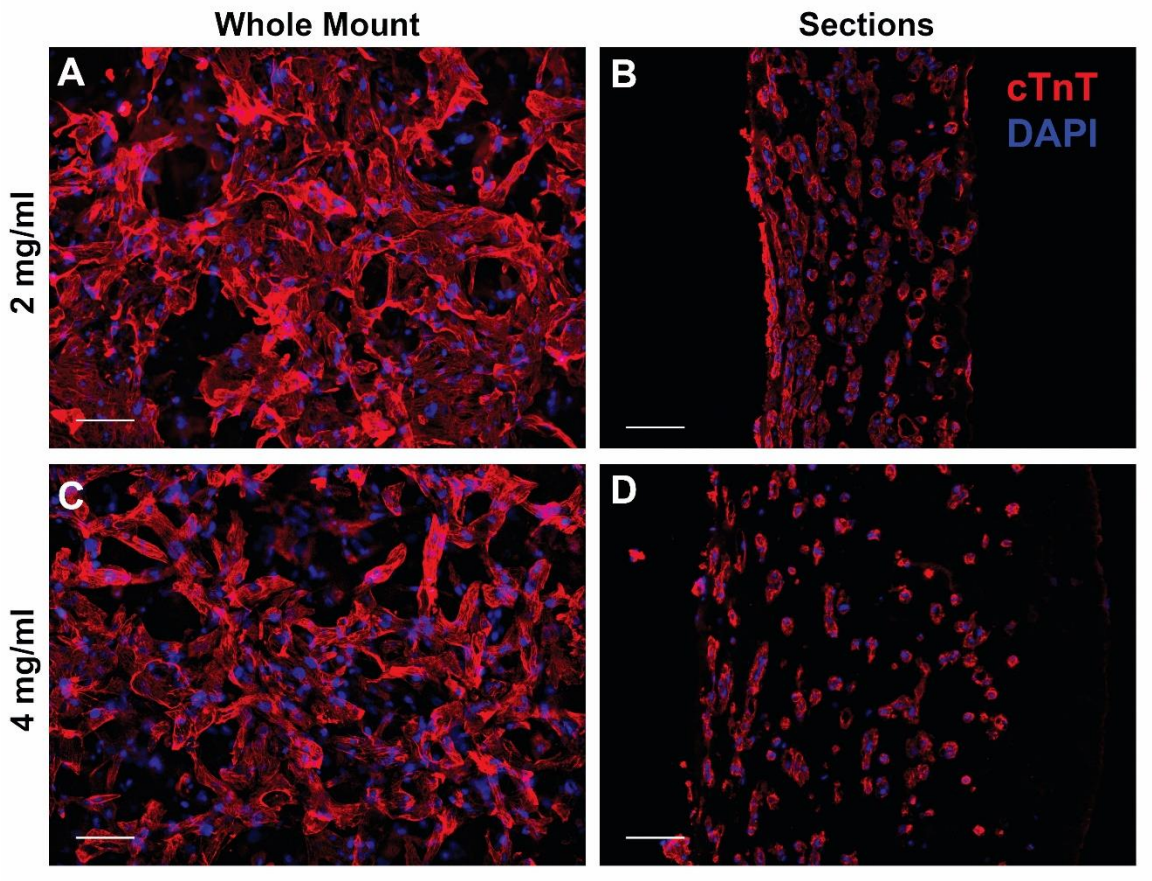

Figure 2-3. Immunofluorescence images of ECTs.

A,C) whole mount and **B,D)** cross-sections of **A,B)** 2 mg/ml and **C,D)** 4 mg/ml ECTs. Whole mount images indicate an isotropic orientation of cells. Cross-sections show the cells oriented within planes parallel to the substrate, particularly near the bottom surface (left side of B,D), consistent with transverse isotropy. Scale bars = 100 μm, red = cTnT, blue = DAPI.

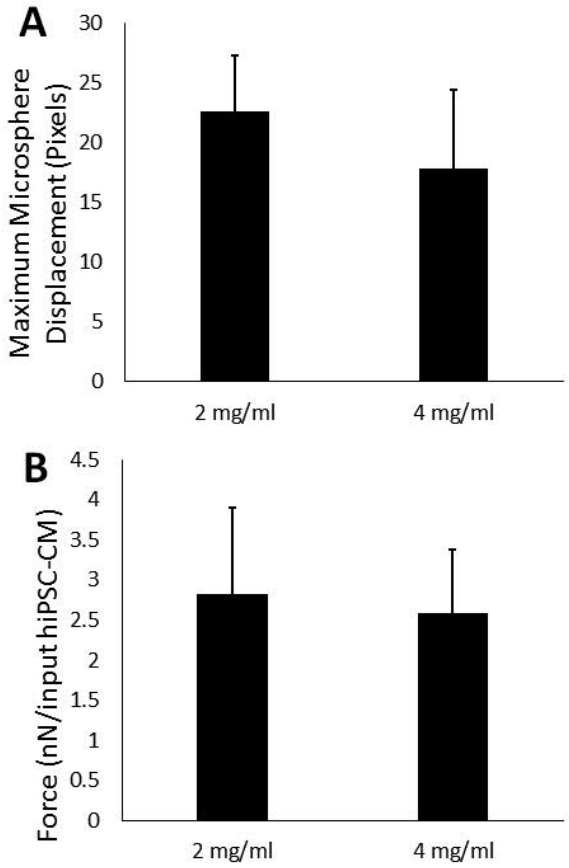

Figure 2-4. Comparison of fibrinogen concentrations.

A) Microsphere displacement and **B)** force generation of ECTs comparing different fibrinogen concentrations. No difference was found between ECTs prepared from 2 mg/ml and 4 mg/ml fibrin in either testing modality (n=3; p=0.37 for HTS, p=0.69 for direct force measurements).

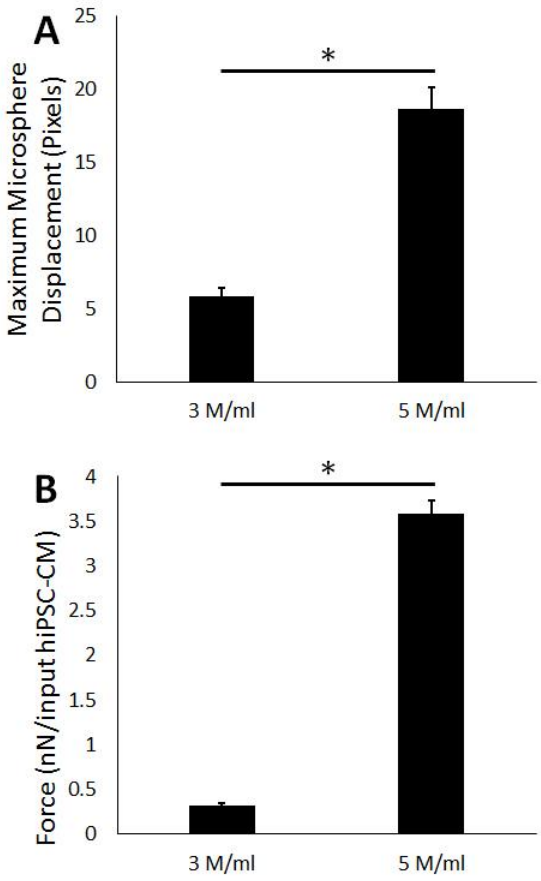

Figure 2-5. Comparison of cell concentrations.

A) Microsphere displacement and **B)** force generation of ECTs comparing different cell concentrations. Both testing modalities showed a difference between the 3 M cells/ml and 5 M cells/ml (n=1; $p<0.05$ for HTS, $p<0.05$ for direct force measurements).

Chapter 3. A cardiac patch from aligned microvessel and cardiomyocyte patches

The material discussed in this chapter is adapted from the following:

Schaefer et al., A cardiac patch from aligned microvessel and cardiomyocyte patches. *Submitted.*

3.1 Abstract

Cardiac tissue engineering aims to produce replacement tissue patches in the lab to replace or treat infarcted myocardium. However, current patches lack pre-formed microvascularization and are therefore limited in thickness and force production. In the present study, we sought to assess whether a bi-layer patch composed of a layer made from human induced pluripotent stem cell-derived cardiomyocytes (hiPSC-CMs) and a microvessel layer composed of self-assembled human blood outgrowth endothelial cells (BOECs) and pericytes (PCs) was capable of engrafting on the epicardial surface of a nude rat infarct model, becoming perfused by the host, and reducing left ventricular (LV) remodeling four weeks after acute implantation. The bi-layer configuration was found to increase the twitch force production, improve hiPSC-CM survival and maturation, and increase patent microvessel lumens compared to time-matched single layer controls after two weeks of *in vitro* culture. Upon implantation, the patch microvessels sprouted into the CM layer of the patch and inosculated with the host vasculature as evidenced by species-specific perfusion labels and erythrocyte staining. The bi-layer patch reduced LV scar wall thinning, but did not improve cardiac functional outcomes compared to control as assessed by echocardiography. Our results demonstrate the added microvessel layer of a bi-layer patch substantially improves *in vitro* functionality, and the bi-layer patch is

capable of engraftment with rapid microvessel inosculation on injured myocardium. The bi-layer format will allow for scaling up in size through the addition of layers to obtain thicker tissues generating greater force in the future.

3.2 Introduction

Coronary heart disease accounts for nearly 1 in 7 deaths each year in the United States [1] with immediate death following myocardial infarction (MI) or progression to heart failure for many survivors. Current treatments are incapable of repairing cellular damage once it has occurred and are limited to preventing further damage and treating symptoms of the disease. The only available method to replace the failing myocardium is by orthotropic heart transplantation; however, this intervention is severely limited by the number of available donor hearts. This treatment deficiency has opened the door for cell- and engineered tissue-based therapies to recover heart function. Direct injections of cells into the infarcted myocardium have shown some success in the clinic. Bone marrow-derived stem cells [3, 4] and skeletal myoblasts [5, 6, 89] have been used in patients with some improvement in terms of wall thickness and ejection fraction. However, cell retention has been low [7] and cardiac arrhythmias have been reported [89]. Cardiac patches constructed using tissue engineering principles are a more reliable cell delivery vehicle for cells since they are associated with a scaffold to ensure their initial retention and survival via a cell niche. They also offer the potential for *in vitro* conditioning, such as mechanical loading [12, 57] or electrical stimulation [58, 59], to improve cellular function and create a functional tissue prior to implantation.

The ultimate goal of cardiac tissue engineering is to fill the need for replacement donor tissues with tissues that can be grown in the lab. One of the main limitations is

sourcing human cells, specifically cardiomyocytes, to use in generating tissues. With the discovery of induced pluripotent stem cells (iPSCs) [90] and the ability to efficiently differentiate functional cardiomyocytes (iPSC-CMs) [18] from them, this need may finally be met. hiPSC-CMs have been used to create patches by entrapment in matrices of primarily collagen [24] and fibrin [25, 58] as well as cell sheets [91] and layer-by-layer [92] methods. A recent study has shown benefit from these tissues in reducing deleterious effects in a rodent model of myocardial infarction [25].

Despite the advances made with cardiac patches, their size is severely limited by their lack of a pre-formed microvasculature to supply nutrients to the tissue. In order to grow tissues that are large enough to generate meaningful force in patients, a method to incorporate a vasculature *in vitro* is required. Previous studies from our group [93] and others [94-96] have shown that engineered human microvessels can become rapidly inosculated and perfused by the host vasculature *in vivo*, including on the epicardial surface following infarction [93]. These studies demonstrate the potential of a patch containing pre-formed microvessels being rapidly perfused once implanted in the host.

The present study reports the creation of bi-layer patch composed of a cardiomyocyte layer (CM) containing human iPSC-CMs and a microvessel layer (BPC) containing human blood outgrowth endothelial cells (BOECs) [97], a circulating endothelial cell type isolated from blood, and human pericytes (PCs), a support cell type that stabilizes microvessels [34]. The two patches are formed separately by entrapping cells in a fibrin gel, and adhered together using fibrin 3-5 days later. Our results here demonstrate the bi-layer patch yields improved contractile function and cell survival, improved CM maturation, and greater microvessel density *in vitro* compared to single-layer time-matched controls.

We have previously demonstrated the BPC patches contained high density microvessel networks [98] that can inosculate with the host vasculature and become perfused with blood in a nude rat acute infarct model after six days [93]. Separately, we have shown that CM patches were able to engraft onto the epicardial surface after myocardial infarction, improve cardiac function, and reduce infarct size after four weeks in the same infarct model [25]. The present study investigated the use of the bi-layer patch made from adhering together and co-culturing a BPC and CM patch, in the same infarct model to determine if it would limit LV remodeling and become perfused *in vivo*. The performance of the bi-layer patch was evaluated with echocardiography to determine cardiac function and histological characterization to determine scar size, patch engraftment, and vascular properties. The patch was tested in both orientations, either with the CM layer or microvessel layer in contact with the epicardial surface and was compared to a CM-only patch.

3.3 Methods

3.3.1 Culture of hBOECs and hPCs

Human BOECS were isolated by the lab of Dr. Robert Hebbel at the University of Minnesota – Twin Cities [97]. Passage 5 BOECs were thawed and plated on 0.05 mg/ml collagen I-coated flasks in BOEC medium (EGM-2 bulletkit medium (Lonza) supplemented with 10% FBS and 1% penicillin/streptomycin (Gibco)). Medium was changed every other day and BOECs were passaged after 4 days, then plated and cultured for 4 days prior to harvest.

GFP-labeled human PCs were obtained from the lab of Dr. George Davis at the University of Missouri. Passage 6 PCs were thawed and plated on 1 mg/ml gelatin-

coated flasks in PC medium (13% FBS, 1% penicillin/streptomycin (Gibco), 10 ng/ml gentamicin (Gibco) in low-glucose DMEM (Lonza)). Medium was changed every 2 days and PCs were harvested after 10 days.

3.3.2 Culture of hiPSC-CMs

Human iPSC-CMs were obtained from the lab of Dr. Timothy Kamp at the University of Wisconsin-Madison. Cells were differentiated via the small molecule Wnt/GSK3 inhibition (GiWi) protocol [18] from hiPSC cell line DF19-9-11T. The purity of the differentiated cells was determined by flow cytometry for cardiac troponin-T (cTnT)+ cells at day 15 of differentiation to be 75-95% cTnT+. Cells were frozen in 90% FBS and 10% DMSO at $10x10^6$ cells/vial and stored in liquid nitrogen before shipping. hiPSC-CMs were thawed into 2 µg/cm2 fibronectin-coated (Sigma) T75 flasks and cultured in 15 ml EB-20 medium (DMEM/F12 basal medium (Corning), 0.1 mM 2-mercaptoethanol (Sigma), 0.1 mM nonessential amino acids (Hyclone), 1 % penicillin/streptomycin (Gibco), and 20% FBS). Medium was replaced 24 hours after thaw to remove any residual DMSO and dead cells and changed to 2% FBS medium (EB-2) 48 hours post thaw. Cells were kept in culture until they resumed beating (approximately 7 days) before harvesting with 0.25% Trypsin/EDTA (Hyclone) + 2% chicken serum (Sigma).

3.3.3 Creation of aligned microvessel patches

Ridges were melted into the bottom of a 6 well tissue culture plate to form rectangular wells measuring 18.4x5 mm. A drop of sterile vacuum grease was applied at each end of the well using a sterile 3 ml syringe and a sterile porous polyethylene spacer (5x5 mm) was placed on top of the grease leaving a well measuring 8.4x5 mm. Droplets

of fibrin gel forming solution containing BOECs and PCs were pipetted onto the inner edge of the spacers and dragged inward to fill the central well. Placing the droplets first is important to ensure the fibrin gel is integrated in the pores of the spacers, anchoring it in place and preventing longitudinal compaction. The fibrin forming solution was composed of 4 mg/ml fibrinogen (Sigma), 200 ng/ml stem cell factor (SCF), interleukin-3 (IL-3), and stromal derived factor 1α (SDF-1α), vascular endothelial growth factor (VEGF), basic fibroblast growth factor (bFGF) (R&D Systems), 1.82 M/ml BOECs, 0.36 M/ml PCs, 1.25 U/ml thrombin (Sigma), and Medium 199 basal medium (Gibco)(M199). The total volume of each gel was 120 µl. Samples were allowed to set in a sterile tissue culture hood for 10 minutes then transferred to a 37°C, 5% CO2 incubator for an additional 15 minutes before covering with 4 ml of BOEC medium + 2 mg/ml ε-aminocaproic acid (ACA) per well. Medium was changed at 24 hours and every other day thereafter.

After 5 days of culture, samples were detached from the bottom of the 6-well plate and carefully transferred to a new well. Spacers were anchored 8.4 mm apart on fresh drops of vacuum grease to maintain sample length. Detachment from the bottom of the well plate allows cell-induced lateral compaction which causes longitudinal alignment of microvessels and fibrin fibrils.

3.3.4 Creation of aligned hiPS-CM patches

Culture wells were created identically to culture wells for aligned microvessel patches, and patches were formed in the same manner. Fibrin gel forming solution was composed of 4 mg/ml fibrinogen, 4 M/ml hiPSC-CMs, 1.25 U/ml thrombin, and M199 basal medium. The total volume of each gel was 120 µl. Samples were allowed to set in

a sterile tissue culture hood for 10 minutes then transferred to a 37°C, 5% CO2 incubator for an additional 15 minutes before covering with 4 ml of EB-20 + ACA medium per well. Medium was changed to EB-2 + ACA fter 24 hours and changed every other day thereafter. hiPSC-CM patches were detached from the bottom of the 6-well plate in the same manner as microvessel patches after 24 hours due to the slower rate of cell-induced compaction of the hiPSC-CM gels.

3.3.5 Bi-layer patch formation

Microvessel and hiPSC-CM patches were cultured statically after detachment for 3-5 days before adhering them together (Figure 3-1). Medium was aspirated from both patches, and replaced with phosphate buffered saline (PBS) for 5 minutes to minimize residual serum left in constructs. Patches were then soaked in 10 mg/ml fibrinogen solution diluted in 20 mM HEPES in 37° C, 5% CO_2 incubator for 20 minutes. The fibrinogen solution was aspirated from the hiPSC-CM patch, and the microvessel patch was cut from its spacers. 10 µl of a 5 U/ml thrombin solution (with 2 mM $CaCl_2$ in DMEM+20 mM HEPES) was added to the surface of the hiPSC-CM patch, and the microvessel patch was carefully placed on top using sterile forceps. Bi-layer patches were allowed to set in the culture hood for 10 minutes, then in 37° C, 5% CO_2 incubator for 20 minutes before addition of EB-20 medium + ACA. Medium was changed to EB-2 + ACA 24 hours later and every other day thereafter. Bi-layer patches were cultured statically for 2 weeks before *in vitro* assessment or *in vivo* implantation.

3.3.6 Patch characterization

Two weeks after creating the bi-layer patches, a subset of patches not to be implanted were fixed with 4% paraformaldehyde (PFA)(Electron Microscopy Sciences) for 1 hour at 4°C followed by rinses with PBS. Samples were cut in half and placed in infiltration solution 1 (30% w/V sucrose in PBS) at 4°C overnight and then transferred to infiltration solution 2 (50% infiltration solution 1, 50% embedding medium (TissueTek OCT)) for 4 hours at room temperature. Samples were frozen in embedding medium and 9 µm sections were cut for immunohistochemical staining. Sections were permeabilized with 0.1% Triton-X100 for 10 minutes, rinsed with PBS three times for 5 minutes each, blocked in 5% normal donkey serum (Jackson Immunoresearch) for 2 hours, and incubated in primary antibodies against specific antigens at 4°C overnight in blocking solution. Sections were rinsed with three 5 minute incubations of PBS before adding secondary antibodies for 1 hour in a solution of Hoescht 33342 diluted 1:10,000 at room temperature. See Table 3-1 for antibody dilutions.

3.3.7 Western Blot

A small sample from the CM-only or delaminated bi-layer patch was digested using NP40 buffer containing protease and phosphatase inhibitors. A reducing SDS-PAGE gel was used to separate 20 g of total protein from these isolates before being transferred to a nitrocellulose membrane (Whatman). Blots were blocked for 1 hour (5% dry milk, 0.1% Tween-20 in PBS), incubated in primary antibody for 1 hour (diluted in TBS-T (Tris buffered saline +0.1% Tween-20)), and washed in TBS-T prior to incubation in HRP-conjugated secondary antibody for 1 hour in blocking solution. Blots were washed with TBS-T and PBS before being developed by with Luminata Classico (Millipore). Films were scanned using HP Deskjet F4400 and quantified using ImageJ

(NIH). Normalization was performed by dividing intensity of protein of interest by the CM protein loading control cardiac troponin-C (cTnC) followed by dividing all sample data by the CM-only value. See Table 3-2 for antibody dilutions.

3.3.8 Experimental design

Four groups were evaluated in this study: 1. MI + bi-layer patch CM side down onto infarct (CM down) (N=7), 2. MI + bi-layer patch microvessel side down onto infarct (BPC down) (N=7), 3. MI + CM patch only (CM-only) (N=6), and 4. MI + empty suture knots in the epicardial surface (sham) (N=8). Both orientations of the bi-layer patch were tested to ascertain any orientation dependence. The CM-only group served as an avascular control. The sham group served as patch free control, while still having the puncture wound and the absorbable sutures used to attach the tissue patches (to control for any effect of the suture degradation products).

3.3.9 Implantation of patches into an acute nude rat infarct model

Procedures used in this study were reviewed and approved by the Institutional Animal Care and Use Committee and Research Animal Resources at the University of Minnesota and conform to NIH guidelines for care and use of laboratory animals.

Twenty-eight female Foxn1rnu nude rats (Envigo) were used in this study, aged 8-9 weeks old and weighing 150-200 g. Isoflurane was administered for anesthesia, and rats were intubated and ventilated for the duration of surgery. The chest was open via sternotomy to expose the heart, and the LAD was permanently ligated to achieve the MI, evident by color change on the epicardial surface. Once established, two patches were cut from the porous spacers and sutured parallel to one another over the infarcted region

for treatment groups. For the sham group, four knots were placed in the epicardium in the approximate location of patch sutures to replicate the puncture wound and suture degradation to which the treatment groups were exposed. After patch placement, the chest was closed and the animals were allowed to recover.

3.3.10 Cardiac functional measurements

Echocardiography (Vevo 2100 system) was conducted prior to implantation and at two follow-up time points: 1 week and 4 weeks post implantation. Ejection fraction and fractional shortening were determined from two long axis and three short axis views from each animal at each time point.

3.3.11 *In vivo* vessel perfusion

After the week four echocardiogram, animals were anesthetized with isoflurane and the chest was reopened. Immediately prior to sacrifice, human and rat specific endothelial labels, rhodamine-conjugated ulex europaeus agglutinin – I (UEA-I)(Vector Laboratories) and fluorescein-conjugated griffonia simplicifolia lectin I, isolectin B4 (IB4)(Vector Laboratories), respectively, were injected into the left ventricle and allowed to circulate for 1 minute. The animal was then euthanized with an intracardiac injection of potassium chloride prior to explanting the heart.

3.3.12 Tissue preparation

After explantation, hearts were rinsed in PBS for 15 minutes before making a single transverse cut directly below the ligation suture. The pieces were then fixed in 4% PFA overnight at 4°C on an orbital shaker. After fixation, another transverse cut was

made halfway between the apex and the first cut. The three pieces were then rinsed in PBS three times for 15 minutes each. Sections were then placed in infiltration solution 1 for 24 hours, followed by infiltration solution 2 for 48 hours at 4°C before freezing in embedding medium. The frozen pieces were cut into 9 µm sections for histological and immunohistochemical analysis.

3.3.13 Infarct assessment

Masson's trichrome stain was used to characterize the infarct size and scar wall thickness. The infarct size was measured in terms of the percent area of the LV free wall occupied by scar. Values for a single animal were determined from transverse sections of the heart. Scar thickness was determined by averaging 9-12 measurements of LV thickness in the region occupied by scar.

3.3.14 Perfusion analysis

Cryosections were fluorescently stained and imaged to visualize all human vessels, as well as perfused human and rat vessels at the time of explantation. Perfused rat vessels were labeled with fluorescein (488 nm excitation) via IB4, perfused human vessels labeled with rhodamine (561 nm excitation) via UEA-1, and all human vessels labeled with Cy5 (647 nm excitation) via hCD31 (Dako) to allow separation of vessel types. The fraction of perfused human vessels was determined by comparing the number of hCD31+ vessels that were co-labeled by the perfusion labels with those that were only hCD31+. Because PCs express GFP, rat perfused vessels and PCs were distinguished by morphology. A green lumen structure was considered a recruited

pericyte if the interior of the lumen contained positive stain for hCD31. All other green lumen-like structures were considered perfused rat vessels.

3.3.15 Cardiomyocyte and vessel alignment characterization

Heart sections were stained for f-actin using rhodamine conjugated phalloidin (Invitrogen) counterstained with hCD31 to detect human microvessels. Cardiomyocyte orientation in the CM layer of the bi-layer patch or CM only patch was analyzed from the f-actin stain using the Measure feature of the OrientationJ plugin [99, 100] for ImageJ. The entire patch was imaged and assembled into a stitched image. Small subsections of the patch were analyzed at a time due to the curvature of the patch on the epicardial surface. Then, the angles of the human and rat vessels were measured in each subsection and compared to the average angle of the cardiomyocytes of that section.

3.3.16 Statistical analysis

Data are represented as mean ± standard deviation. Students t-tests were performed in Excel. Multiple groups were compared with 1-way analysis of variance (ANOVA) with Tukey's HSD post-hoc tests in Minitab or IBM SPSS. P-values < 0.05 were considered significant.

3.4 Results

3.4.1 *In vitro* characterization

Both the CM-only and BPC-only patches became aligned via cell-induced vertical compaction from time of casting and lateral compaction after the gels were detached from the bottom surface of the culture plate. Final patch dimensions are listed in Table

3-3. Longitudinal sectioning of the bi-layer patch at the end of the additional two weeks of culture following adherence of CM-only and BPC-only patches together revealed that alignment was maintained in both the CM and BPC layers (Figure 3-2B). The final CM density was measured from cross-sectional views of the patches. After two weeks, the density was significantly greater in the CM layer of the bi-layer patch compared to a time-matched CM-only patch (237.0 ± 10.7 vs. 35.2 ± 9.4 CM/mm^2, $p<0.05$) (Figure 3-2C-D). Assuming that cells were evenly distributed throughout the construct at the time of casting, and limited cell migration, the approximate total CM count was estimated based on the number of cells in a cross sectional slice. This results in count estimates of 497k ± 35k vs 146k ± 44k for the bi-layer patch and CM-only patch, respectively.

Cross-sections were also used to investigate the health of the microvessels two weeks after forming the bi-layer patches. The bi-layer patches maintained lumens in the BPC layer (Figure 3-2A). Final lumen density was compared between the BPC layer of the bi-layer patch and time-matched single layer BPC patches. The bi-layer patches contained more lumens than the BPC-only control (34 ± 12 vs 7 ± 3 lumens/mm^2, $p<0.05$).

Both CM-only patches and bi-layer patches beat spontaneously and produced measureable twitch forces when paced with field stimulation. The force of the bi-layer patch increased between one and two weeks, whereas the CM-only patches did not show improvement with time. At both one week and two weeks post adhering, the bi-layer patches produced more force than the CM-only controls. These differences were true when comparing both the force and the force normalized to the number of input CMs at the time of sample casting (Figure 3-3, $p<0.05$). The force per input CM has

been proposed as a measure of the of "patch efficiency" [27] as it attempts to incorporate how the final functional output is affected by the input conditions.

Western blot analysis of the CM-only and CM layer of the bi-layer patch was conducted to determine potential differences in CM maturation during *in vitro* culture. The primary focus was to compare the ratio of the mature isoform cTnI to the immature isoform ssTnI, as proposed previously [101]. This has been suggested as better maturation marker as the conversion from ssTnI to cTnI is complete, with the adult CMs containing only cTnI [102, 103]. This conversion is non-reversible in stress or disease conditions [103, 104], unlike other common maturation markers. SERCA2A, a calcium pump on the sarcoplasmic reticulum, was also investigated. It was found that the cTnI:ssTnI ratio was approximately 3-fold higher in the bi-layer patch than in CM-only patch; however, there was no difference in SERCA2A expression (Figure 3-4).

3.4.2 Patch engraftment

The patches characterized above (Figure 3-5A) were implanted acutely onto infarcted rat hearts (Figure 3-5B). Four weeks after implantation, the epicardial surface was covered with a thin, white layer of tissue covering most of the LV surface. After assessment, this layer was found to be patch surrounded by scar tissue (Figure 3-6A). The patch was found to be composed of CMs packed too densely to identify individual cells. We have shown previously in this model by counterstain with human nuclear antigen that these are iPS-CMs [25]. At high magnification, sarcomeric banding could be easily seen in these CMs (Figure 3-6C). The patches ranged from 200-250 μm thick on the epicardial surface, but there were no differences in thickness between groups (Figure 3-6B). While the CM layer of the bi-layer patch and the CM-only patch were

found in all animals, the BPC layer of the bi-layer patch was rarely found after four weeks *in vivo*. Staining for f-actin and examination of orientation revealed the CMs were aligned circumferentially around the heart (Figure 3-6D). This is consistent with the orientation of the aligned patches upon implantation (Figure 3-5B).

3.4.3 *In vivo* vessel characterization and perfusion assessment

The total number of human microvessels as well as the number of perfused human and rat vessels that sprouted into the CM layer of the bi-layer patch and into the CM-only patch were quantified (Figure 3-7). Staining with human-specific CD31 (hCD31) antibody revealed no difference in the total number of human vessels between the two orientations of the bi-layer patch (65 ± 55.1 vs 48 ± 52 vessels/mm^2, CM down and BPC down, respectively). The percent of perfused human vessels was determined by comparing the co-localization of the UEA-I label injected prior to sacrifice and hCD31. Perfusion was verified by immunofluorescence stain for rat RBCs (Figure 3-8A). One animal that died at two weeks post-implantation contained human microvessels throughout the thickness of the CM layer that were filled with blood (Figure 3-8B). There was no difference in the perfused fraction of the human vessels in either orientation of the bi-layer patch (67 ± 28% vs 53 ± 33%, CM down and BPC down, respectively). Perfused rat vessels in the CM layer of the bi-layer patches or CM-only patch were quantified using the perfusion label IB4. Similarly, there was no difference between any of the groups (104 ± 52, 44 ±23, 96 ±61 vessels/mm^2 for CM-only, CM down, and BPC down respectively). The total number of vessels, human and perfused rat, was not different between groups either (104 ± 52, 108 ± 70, 144 ± 66 vessels/mm^2; CM-only, CM down, BPC down, respectively).

The alignment of rat and human vessels (Figure 3-6D) of a subset of animals (N=4) was measured relative to the local CM alignment determined with f-actin staining. The difference in mean angle alignment was 5.8 ± 40.2° for human vessels and 12.1 ± 39.0° for rat vessels indicating strong co-alignment of the microvessels growing into the aligned CM layer.

3.4.4 Left ventricle remodeling

The extent of LV remodeling was determined using Masson's trichrome staining. The size of the scar four weeks after surgery as a function of LV free wall area occupied by scar, and the thickness of the scar are summarized in Figure 3-9. The patch was excluded from these measurements when identified (e.g. Figure 3-6A). No difference was observed in the percent area of the scar between any of the implant groups and sham group (30.6 ± 6.2%, 37.6 ± 10.3%, 36.2 ± 5.4%, 37.4 ± 7.7% for CM down, BPC down, CM-only, and sham, respectively). However, the scar thickness in the bi-layer patch groups (CM down and BPC down) were thicker than the sham group (1443 ± 511 μm and 1403 ± 360 μm vs 862 ± 84 μm, respectively, $p<0.05$), whereas the CM-only group was not different than sham (1200 ± 363 μm vs 862 ± 84 μm, respectively).

3.4.5 Cardiac functional changes

Cardiac function was assessed using echocardiography. Long- and short-axis echocardiograms were collected prior to infarction and post-infarction at 1 and 4 weeks. Ejection fraction and fractional shortening were calculated at each time point (Figure 3-10). No difference was found in either measurement between any of the groups and sham.

3.5 Discussion

This study demonstrated that adhering a hiPS-CM patch and a human microvessel patch together with fibrin results in a human bi-layer cardiac patch that, after two weeks *in vitro*, produces substantially greater twitch force, greater CM survival, and enhanced CM maturation compared to a CM-only control patch. After four weeks *in vivo*, the microvessels from the BPC layer of the patch were able to migrate into the CM portion of the patch, become inosculated with the host vasculature, and perfused with blood. Our previous studies have demonstrated the beneficial effect of CM patches acutely placed on the epicardial surface of an infarcted rat heart [12, 25]. We have also previously shown in the same model that microvessel patches implanted on infarcted epicardium become inosculated with the host vasculature after 6 days and perfused with blood [93]. The present study focused on combining a CM patch with a microvessel patch that could rapidly be perfused *in vivo*.

The bi-layer patch format provided benefit to both layers of the patch. The mechanism behind this benefit is uncertain; however, the functional outcomes are clear. Both bi-layer and CM-only patches exhibited measurable twitch forces. The CM-only patches (0.3 nN/input CM) of the present study, which were made directly from the differentiated hiPSC, were similar to our previously reported hiPSC-CM+PC patches (0.2 nN/input CM)[25], where we purified the differentiated hiPSC for CM and replaced the non-CM fraction with hPC. The bi-layer patches (2.17 nN/input CM) were an improvement over our previously reported patches made from neonatal rat heart isolates (1.2 nN/input CM) [12], although less contractile than patches made from hESC-CMs (5.7 nN/input CM) [27]. The reason for the nearly 10-fold increased twitch force observed in the bi-layer patch

compared to the CM-only patch appears to have two causes. First, the number of CMs at the time of force testing was greater in the bi-layer patches. It has been shown that endothelial cells protect CMs from apoptosis, potentially through neuroregulins [105] or PDGF [106] pathways. While the difference in cell number certainly contributed to the difference in twitch force, the twitch force produced by the bi-layer patch was nearly 7.5x that of the CM-only patch, while the final bi-layer patch CM count was only 3.4x that of the CM-only patch. The second factor is apparent increased maturation of the CMs in the bi-layer patch. It has been shown in mice that the force produced by cardiomyocytes increases with age from the embryonic to adult phenotype [107]. The 3-fold increased ratio of cTnI:ssTnI in the bi-layer patch CMs indicates a switch to a more mature phenotype in the present study. As the replacement of ssTnI with cTnI is irreversible and complete in the adult CM [102, 103, 107], the bi-layer patch format confers CM maturation that is absent in the CM-only patch. The benefit to the BPC layer of the bi-layer patch is the increase in observed microvessel lumens. This could be due to reduced compaction of the BPC layer of the bi-layer patch because it was “fixed” on the bottom surface to the CM layer, or to a diffusible factor released in the CM layer that is inhibitory to compaction induced by the PCs or BOECs. Excessive compaction of the fibrin gel can lead to collapse of microvessel lumens [9].

After two weeks of *in vitro* culture, the two layers of the bi-layer patch were well integrated. Some of the supporting PCs were able to migrate across the interface between the two layers, but no microvessels migrated into the CM layer prior to implantation. However, we did find extensive microvessel sprouting into the CM layer of the patch after four weeks *in vivo*. More importantly, a large portion of the human microvessels had inosculated with the host vasculature and become perfused. This is a

promising result for future studies with thicker patches that can generate physiologically-relevant force as it will be imperative to establish perfusion of the patch quickly to prevent necrosis. As evidenced by one animal that died two weeks after implantation, microvessel sprouting throughout the full thickness of the CM layer, including perfusion of the vessels with blood (Figure 3-8B), can occur in as little as two weeks, indicating sprouting into the CM layer was rapid after implantation. The microvascular remodeling of the patch that occurred *in vivo* was most likely caused by the drastically different microenvironment in the hypoxic and nutrient-deficient infarct region. The bi-layer patches were relatively thin, and adequately supplied with nutrients and oxygen *in vitro* solely by diffusion from the surrounding culture medium, as no necrotic regions were observed. Once implanted, the CMs likely experienced stress from the lack of a nutrient rich medium bath and released angiogenic factors, potentially through exosomes [108]. It has also been shown that global expression of vascular endothelial growth factor (VEGF), a potent angiogenic factor, is increased in the myocardium following ischemia [109].

Both human and rat microvessels that migrated into the CM layer and CM-only patch were found to co-align with the implanted CMs. This co-alignment was likely caused by cell contact guidance, where cells preferentially migrate bidirectionally in response to aligned extracellular matrix fibrils [110]. This has been demonstrated with endothelial cells in collagen-nanofiber hydrogels [111] and fibrin hydrogels [112]. In the present study, the patch was primarily aligned fibrin at the time of implantation. The sprouting endothelial cells may have followed these fibrin fibrils as they migrated into the CM layer of the patch. Cell-produced ECM post-implantation or the aligned CMs may also have provided contact guidance cues for the migrating endothelial cells.

The cardiac functional results from this study did not match the benefit seen in our previous work [12, 25]. However, the procedure for adhering the microvessel layer to the CM layer necessitated changing how the CM layer was formed. Previously, a tubular mold was used to make an aligned ring construct cut into three patches that were sutured onto the epicardium [12, 25]. The slab format used in the present study resulted in a smaller patch, with fewer than half of the total CMs delivered to the epicardium compared to our previous study. This reduction in cell content would greatly reduce the amount of any paracrine signals released from the patch that could have a beneficial effect on the surrounding myocardium, as neither mechanical support nor electrical coupling and contractile support were implicated in the functional beneficial effect seen previously [25].

Future studies could be directed at trying to simulate the infarcted environment *in vitro* to induce vessel formation into the CM layer. One way to accomplish this might be through the use of a hypoxic incubator. The reduced oxygen would simulate the stress that the CMs experience in the infarct region from reduced blood flow. A method to induce local hypoxia in the CM patch could be to increase the metabolic activity of the CMs by introducing a drug that increases contraction rate, such as isoproterenol, or through the use of electrical stimulation during *in vitro* culture. Electrical stimulation also has been shown to improve functional outcomes of CMs including increased force production [58] and CM maturation [59].

Preliminary studies involving triculture of hiPSC-CMs, BOECs, and PCs were unable to produce any microvessel formation (data not shown), leading to the development of the bi-layer patch. While this approach yields an engineered cardiac tissue in close proximity to a microvessel network, the final patch thickness remains too

small for use beyond a rodent model. In the future, multiple bi-layer patches could be adhered together using the same method to create a thicker patch that generates physiologically relevant force. By creating a thicker tissue, one could also better simulate *in vitro* the stressed environment the CMs experience *in vivo*, which could lead to microvessels sprouting into the CM layers prior to implantation. Attaching the microvessel patch to an external perfusion pump, preferably through a larger diameter vessel integrated into the microvessel patch, could also help induce sprouting into the CM patch. Previous studies have shown the benefit of flow for improving microvessel network properties [9, 113].

3.6 Conclusion

We created a bi-layer cardiac patch made from an hiPSC-CM layer and a self-assembled human microvessel layer. After two weeks of culture, this arrangement led to increased force production, CM survival and maturation, and microvessel density when compared to time-matched single-layer controls. Upon implantation into a nude rat acute myocardial infarction model for four weeks, the bi-layer patches reduced LV wall thinning compared to sham animals. The CM layer of the bi-layer patches became dense and was invaded by human and rat microvessels that were co-aligned with the CMs and perfused by the host. We believe this study demonstrates a potential method to produce thicker, more contractile patches in the future by increasing the number of layers adhered together.

3.7 Acknowledgements

This work was supported by NIH Grant R01 HL108670 (to R.T.T). We thank Susan Saunders and Jackson Baril for their technical assistance.

3.8 Figures and Tables

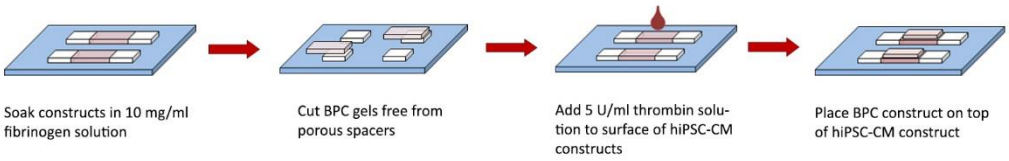

Figure 3-1. Schematic depiction of the bi-layer patch formation.

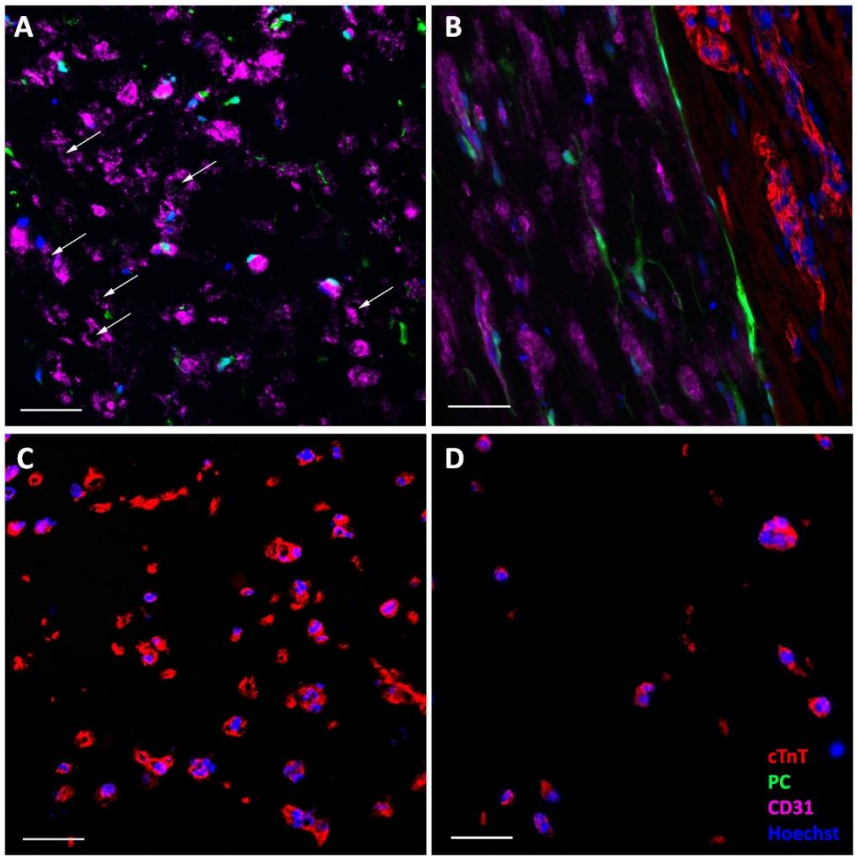

Figure 3-2. Immunofluorescence characterization of patches before implantation. **A)** Cross-section of BPC layer of bi-layer patch. White arrows indicating microvessel lumens. **B)** Longitudinal section of bi-layer patch showing interface between the two layers and the alignment of both CMs (cTnT) and microvessels (CD31). **C)** Cross-sectional view of CM layer of bi-layer patch compared to time-matched **D)** cross-sectional view of CM-only patch. Abbreviations: cTnT, cardiac troponin-T; PC, pericytes. Color of labels is consistent in all panels. Scale bars = 50 µm.

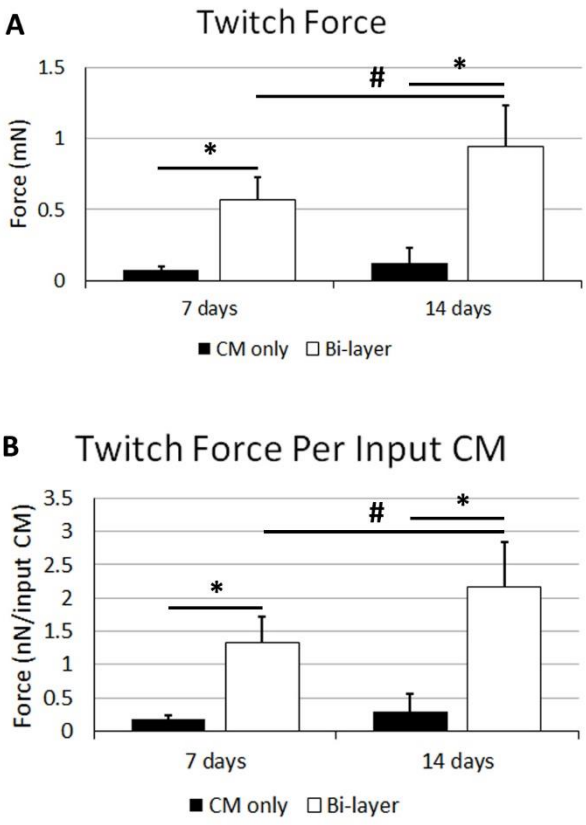

Figure 3-3. Twitch force characterization of patches before implantation.
Twitch force **A)** and twitch force normalized to the number of CMs seeded into the gels during gel formation **B)**. Significance is indicated by horizontal bars between groups, $p<0.05$.

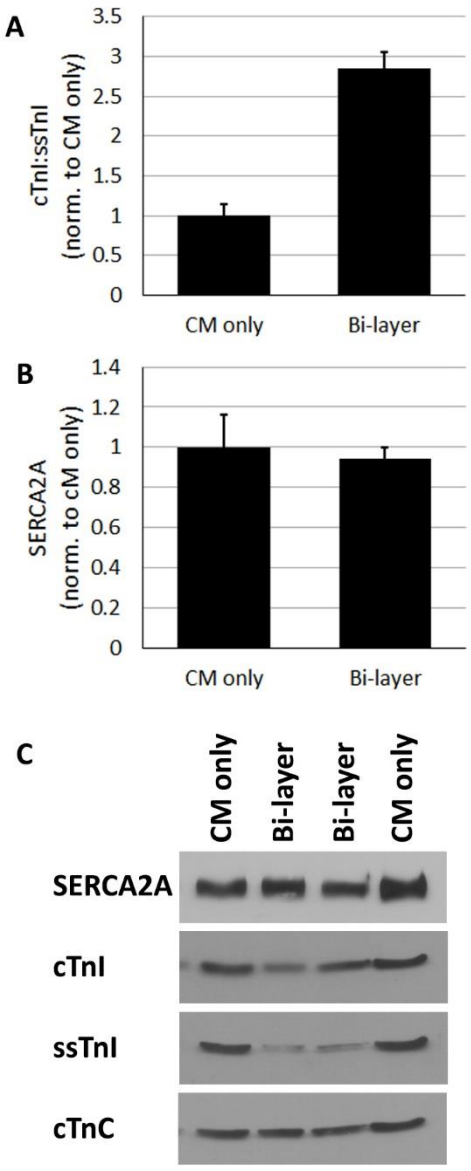

Figure 3-4. Characterization of Western Blot analysis of CM patches. Quantification of bands for **A)** ratio of cTnI:ssTnI, and **B)** SERCA2A. In both cases, values were normalized to the CM-only patch. **C)** Visualization of bands from the scanned films. N=2, error bars indicate range.

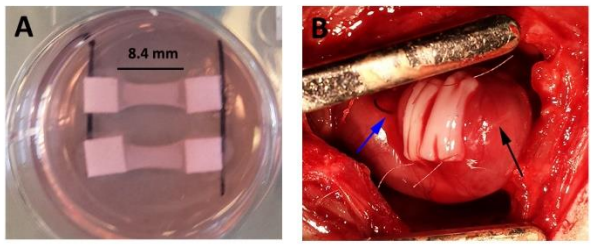

Figure 3-5. Bi-layer patches at implantation.

A) Patches prior to removing from spacers after two weeks of culture. **B)** Two patches sutured onto the left ventricular epicardial surface after myocardial infarction. Blue arrow indicates ligation suture, black arrow indicates apex of heart.

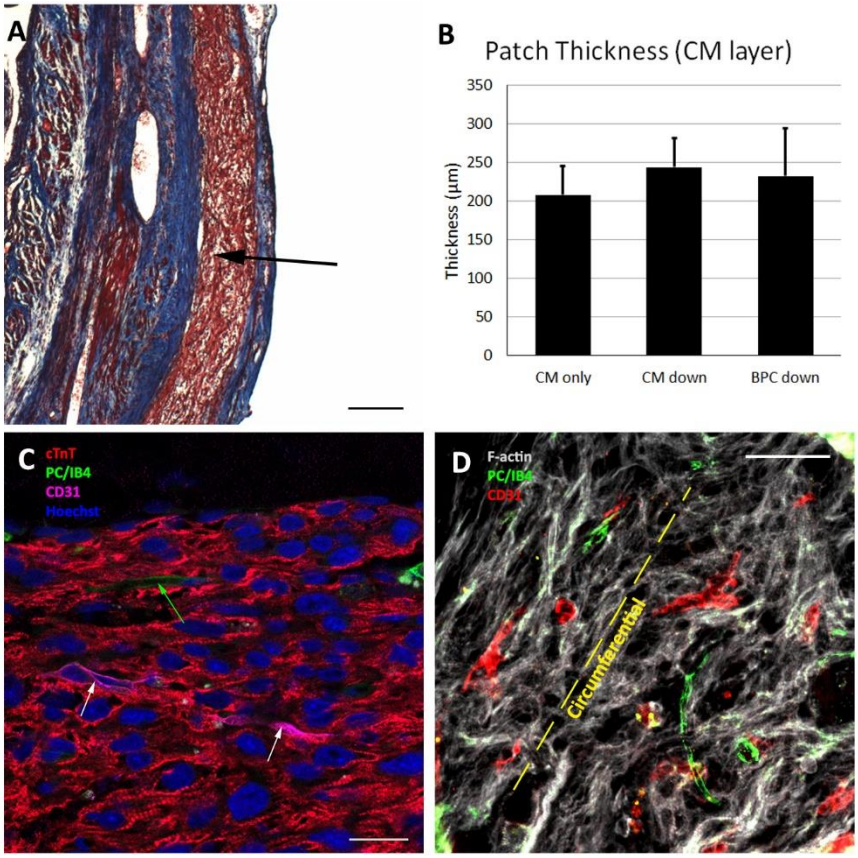

Figure 3-6. Patch engraftment four weeks after implantation.

A) Masson's trichrome image showing patch on the epicardium (arrow). Scale bar = 200 µm. **B)** Patch thickness for each of the three implant groups, where "CM down" and "BPC down" refers to the orientation of the implanted bi-layer patches. **C)** High magnification image of patch showing dense CM layer and sarcomeric banding. White arrows indicate human microvessels and green arrow indicates rat microvessel that have sprouted into the CM patch. Scale bar = 20 µm **D)** F-actin stain indicating alignment of CMs in the circumferential direction. Rat and human microvessels generally co-align with the CMs. Scale bar = 50 µm. Abbreviations: cTnT, cardiac troponin-T; PC, pericytes; IB4, fluorescein conjugated griffonia simplicifolia I, isolectin B4.

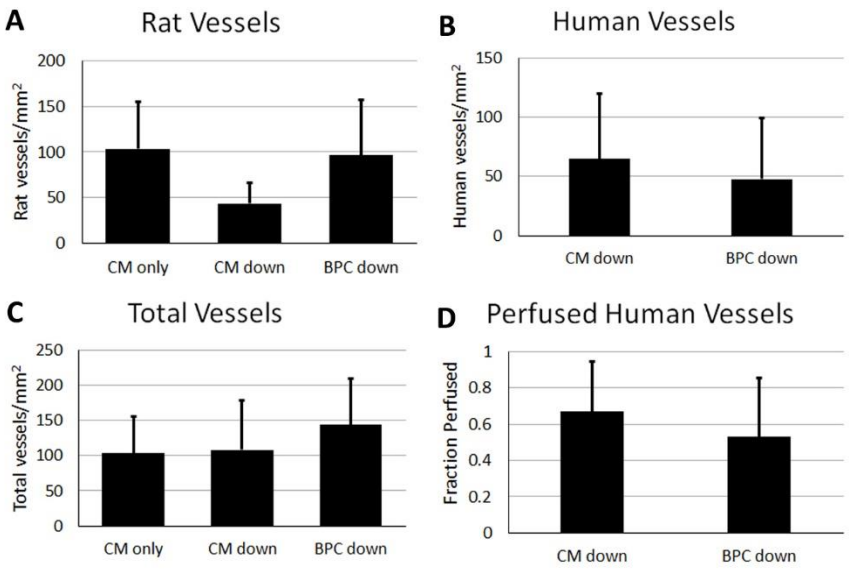

Figure 3-7. Quantification of microvessels *in vivo.*

A) Rat, **B)** human, and **C)** total vessels that sprouted into the CM layer of the bi-layer patch or CM-only patch. **D)** The fraction of human vessels that were perfused at time of explant based on co-localization of CD31 and human perfusion label.

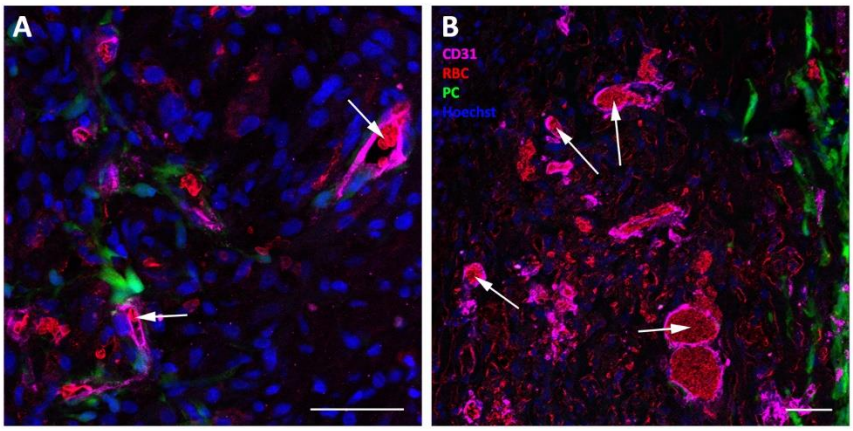

Figure 3-8. Verification of perfusion with rat RBC stain.

A) High magnification view of human microvessels filled with blood after four weeks. Arrows indicate RBCs. **B)** RBCs in human microvessels after two weeks in animal that died prior to completion of study. Scale bars = 50 µm.

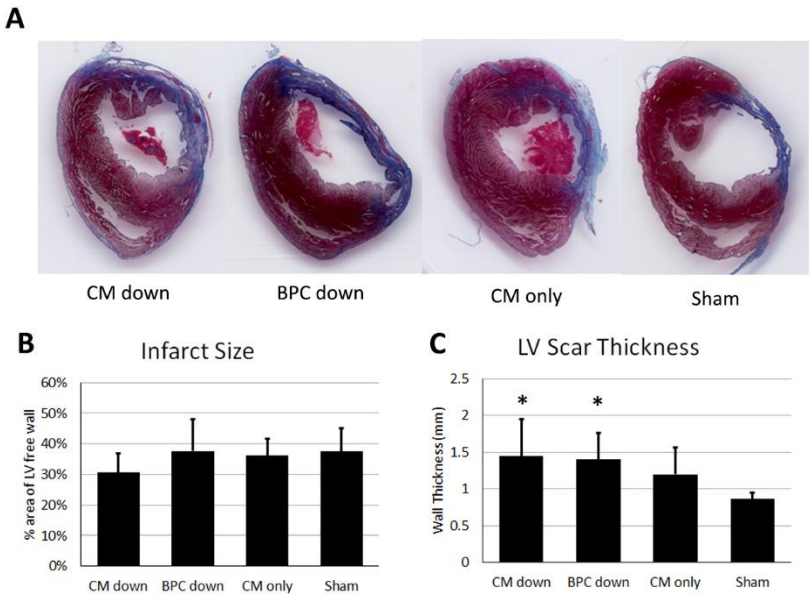

Figure 3-9. Characterization of scar.

A) Representative images of the LV scar from the four groups. **B)** Scar size in terms of the percent area of the LV free wall it occupies. **C)** LV wall scar thickness. * indicate significantly difference than sham, $p<0.05$.

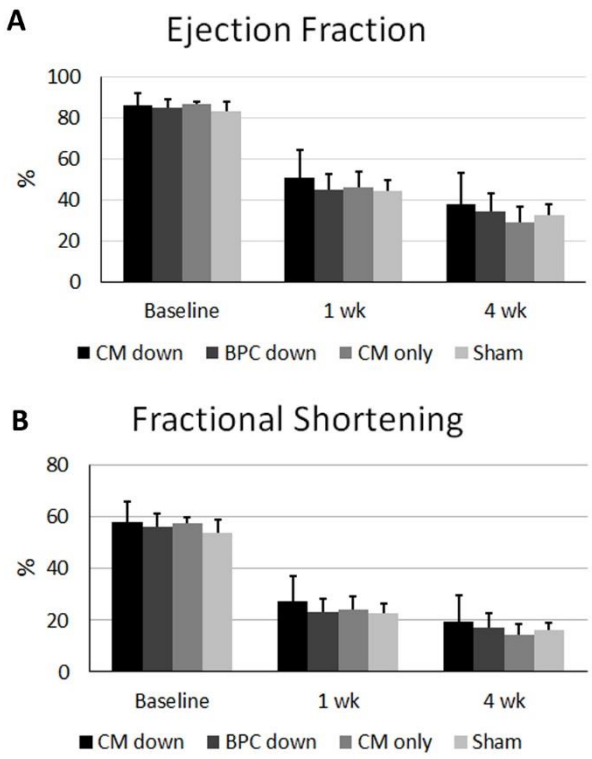

Figure 3-10. Cardiac functional data.

A) Ejection fraction and **B)** fractional shortening for all groups at baseline, 1 week post infarction, and 4 weeks post infarction.

Primary Antibody	Manufacturer	Catalog #	Dilution
Mouse cardiac troponin-T	Thermo Fisher Scientific	MS-295-P1	1:100
Rabbit cardiac troponin-T	Abcam	Ab45932	1:500
Mouse hCD31	Dako	M0823	1:40
Secondary Antibody			
Alexa Fluor 594 AffiniPure Donkey Anti-Rabbit IgG (H+L)	Jackson ImmunoResearch	711-585-152	1:200
Alexa Fluor 594 AffiniPure Donkey Anti-Mouse IgG (H+L)	Jackson ImmunoResearch	715-585-151	1:200
Alexa Fluor 647 AffiniPure Donkey Anti-Rabbit IgG (H+L)	Jackson ImmunoResearch	711-605-152	1:200
Alexa Fluor 647 AffiniPure Donkey Anti-Mouse IgG (H+L)	Jackson ImmunoResearch	715-605-151	1:200

Table 3-1. Antibodies used for immunohistochemistry.

Primary Antibody	Manufacturer	Catalog #	Dilution
Cardiac troponin-I	Millipore	MAB1691	1:1500
Troponin I-SS	Santa Cruz	sc-20645	1:2000
Cardiac troponin-C	Abcam	ab8285	1:2000
SERCA2A	Abcam	ab2861	1:2000
Secondary Antibody			
ECL Rabbit IgG, HRP-linked whole Ab from donkey	GE Healthcare Life Sciences	NA934V	1:2000
ECL Mouse IgG, HRP-linked whole Ab from sheep	GE Healthcare Life Sciences	NA931V	1:2000

Table 3-2. Antibodies used for Western Blotting.

	Length	Total Height	Total Width	BPC Height	BPC Width	CM Height	CM Width
CM-only	8.4[a]	-	-	-	-	1.4±0.2	3.7±0.1
BPC-only	8.4[a]	-	-	0.7±0.2	1.5±0.5	-	-
Bi-layer	8.4[a]	1.8±0.2	2.8±0.3	0.7±0.1	2.2±0.2[b]	0.9±0.1[b]	2.7±0.2[b]

Table 3-3. Patch dimensions prior to implantation.

[a] indicates a constrained direction. Dimensions represented as mean ± standard deviation. Student's t-test comparing patch dimensions between single-layer control and bi-layer halves revealed significant differences (indicated by [b], $p<0.05$) between the CM layer in both the width and height dimensions, and only in the width of the BPC layer.

Chapter 4. Conclusions

4.1 Major Contributions

The work presented in this dissertation has contributed significantly to myocardial tissue engineering. One manuscript has been published and one is in preparation, as well as a number of posters and oral presentations at international conferences and workshops. The major conclusions and relevance to the current state of the field are summarized here.

4.1.1 High throughput screening system for characterization of engineered cardiac tissues

Prior to this work, characterization of engineered cardiac tissues (ECTs) in most laboratories required the creation of centimeter-scale ring-shaped tissues that would be attached to a force transducer for analysis. This process was resource-expensive in terms of cells and materials. Chapter 2 describes the development of an alternative, high throughput system that utilizes a soft polydimethylsiloxane (PDMS) substrate containing fluorescent microbeads for comparing the relative contractile strength of ECTs. Small constructs are formed directly on the surface of the PDMS and microbead displacements can then be captured using a fluorescent microscope while under electric field stimulation. Analysis of the displacements allows for determination of construct conditions that yield greater contractile function. This method does not require highly specialized equipment, can be applied to any contractile tissue, and can be used to test a variety of gel and cell parameters as well as medium supplements.

4.1.2 Creation of a bi-layer engineered cardiac tissue from induced pluripotent stem cell-derived cardiomyocyte (hiPSC-CM) and microvessel patches with improved function and maturity

After optimizing construct conditions for the hiPSC-CM construct using the system described in Chapter 2, this work developed a method for combining hiPSC-CM constructs with a microvessel construct that was previously described by our laboratory[9, 93]. It was determined that soaking the two constructs in fibrinogen solution and then adding thrombin at the interface allows the hiPSC-CM and microvessel constructs to be adhered together. The resulting bi-layer patch leads to over 7-fold increase in the measured twitch force per input cardiomyocyte, increased cell survival, and increased CM maturation compared to control CM-only patches after two weeks *in vitro*. The bi-layer format also helped to maintain patent lumens in the microvessel layer of the patch compared to control microvessel-only patches.

4.1.3 Acute implantation of a bi-layer engineered cardiac tissue engrafts in a nude rat model of myocardial infarction and becomes perfused

After characterization of the bi-layer patch *in vitro*, this work assessed the ability of the patch to engraft, become perfused, and reduce post-infarction remodeling. Results demonstrated that the patches survive and become a dense layer of CMs on the epicardium four weeks after transplantation. Moreover, sprouting occurred from the microvessel layer into the CM layer with a majority of the vessels (53-67%) becoming perfused, regardless of patch orientation. The microvessels that sprouted into the CM layer were also co-aligned with the hiPSC-CMs presumably due to cell contact guidance.

While no functional benefit was observed, the bi-layer patch, in either orientation, was shown to reduce LV scar wall thinning compared to untreated infarcts.

4.2 Future Directions

Although the findings of this work represent significant progress, these bi-layer tissues are still thin and further development is required to bring a vascularized engineered cardiac tissue towards clinical relevance.

4.2.1 Determination of secreted factors responsible for hiPSC-CM survival and maturation in the bi-layer patch

The improvement in the contractile function of the bi-layer patch is clear as are changes in the CM layer that are likely responsible for that improvement. Although potential paracrine signaling mechanisms were proposed in Chapter 3, further experimentation is required to confirm the cause of these improvements. Elucidating the mechanism responsible could have far reaching consequences on the field of myocardial tissue engineering. Once the factor or factors responsible are determined, further investigation may provide an additional means of improving hiPSC-CM maturation broadly applicable to myocardial tissue engineering as well as to the bi-layer patch format. In addition, media supplementation with these factors during *in vitro* culture of the bi-layer patch could potentially improve the tissue beyond the benefit caused by cell-based release. As these studies were only conducted with one BOEC donor, potential variation in expression levels between donors is unknown, and may necessitate *in vitro* supplementation to maintain functional improvement.

Precise determination of these factors may be difficult. Initial studies should be directed at transcriptional changes via RNA sequencing of each layer of the bi-layer patches. This technique allows for investigation of a large parameter space and for quick identification of complementary changes occurring within the construct, for example, the detection of the upregulation of secreted factors involved with CM survival or maturation pathways and the concomitant upregulation of related receptors in the CM-layer.

4.2.2 Establish *in vitro* perfusion of the microvessel layer of the bi-layer patch

The bi-layer format allows for the generation of a patch containing CMs close to an established microvessel network. However, these vessels were not perfused *in vitro* prior to implantation into the animal model. Fortunately, the bi-layer patch was thin enough that culture medium was able to sustain cell metabolism solely by diffusion *in vitro*. In order to generate thicker patches able to produce physiologically-relevant contractile force, multiple layers of bi-layer patches adhered together are envisioned. This will require that the microvessel layers be perfused *in vitro* and/or immediately post-implantation to overcome the limits of diffusion.

Attaining perfusion *in vitro* could be accomplished by connecting the microvessel patch to small diameter vessels at each end, and work towards this goal has already begun in our laboratory. This method would not only allow for perfusion of patches *in vitro*, but also allow the larger vessels to be sutured directly to the host vasculature upon implantation into an animal model, eliminating the time needed for vessel inosculation and minimizing potential cell loss.

4.2.3 Generation of a large multi-layered patch for large animal preclinical models

Once *in vitro* perfusion has been attained, scaling up the size of the patch through the addition of more layers would allow investigation in larger animal models, such as a porcine model of myocardial infarction. However, the size of the individual patches will first need to be increased. An initial patch size measuring 8.4x5 mm is far too small for use in swine. This could be accomplished simply by increasing the size of the initial slab gel that was used in Chapter 3. Through the use of larger individual patches and multiple alternating layers of hiPSC-CMs patches and perfused microvessel patches, a thick, vascularized engineered cardiac tissue could be constructed.

References

1. Mozaffarian, D., Benjamin, E. J., Go, A. S., et al. Heart Disease and Stroke Statistics-2016 Update: A Report From the American Heart Association. Circulation 2016; 133: e38-e360.
2. Caulfield, J. B., Leinbach, R. and Gold, H. The relationship of myocardial infarct size and prognosis. Circulation 1976; 53: I141-4.
3. Suncion, V. Y., Ghersin, E., Fishman, J. E., et al. Does transendocardial injection of mesenchymal stem cells improve myocardial function locally or globally?: An analysis from the Percutaneous Stem Cell Injection Delivery Effects on Neomyogenesis (POSEIDON) randomized trial. Circ Res 2014; 114: 1292-1301.
4. Williams, A. R., Trachtenberg, B., Velazquez, D. L., et al. Intramyocardial stem cell injection in patients with ischemic cardiomyopathy: functional recovery and reverse remodeling. Circ Res 2011; 108: 792-796.
5. Herreros, J., Prosper, F., Perez, A., et al. Autologous intramyocardial injection of cultured skeletal muscle-derived stem cells in patients with non-acute myocardial infarction. Eur Heart J 2003; 24: 2012-2020.
6. Smits, P. C., van Geuns, R. J., Poldermans, D., et al. Catheter-based intramyocardial injection of autologous skeletal myoblasts as a primary treatment of ischemic heart failure: clinical experience with six-month follow-up. J Am Coll Cardiol 2003; 42: 2063-2069.
7. Terrovitis, J., Lautamaki, R., Bonios, M., et al. Noninvasive quantification and optimization of acute cell retention by in vivo positron emission tomography after intramyocardial cardiac-derived stem cell delivery. J Am Coll Cardiol 2009; 54: 1619-1626.
8. Rakusan, K., Flanagan, M. F., Geva, T., et al. Morphometry of human coronary capillaries during normal growth and the effect of age in left ventricular pressure-overload hypertrophy. Circulation 1992; 86: 38-46.
9. Morin, K. T., Dries-Devlin, J. L. and Tranquillo, R. T. Engineered microvessels with strong alignment and high lumen density via cell-induced fibrin gel compaction and interstitial flow. Tissue Eng Part A 2014; 20: 553-565.
10. Black, L. D., 3rd, Meyers, J. D., Weinbaum, J. S., et al. Cell-induced alignment augments twitch force in fibrin gel-based engineered myocardium via gap junction modification. Tissue Eng Part A 2009; 15: 3099-108.
11. Brown, M. A., Iyer, R. K. and Radisic, M. Pulsatile perfusion bioreactor for cardiac tissue engineering. Biotechnol Prog 2008; 24: 907-20.
12. Wendel, J. S., Ye, L., Zhang, P., et al. Functional consequences of a tissue-engineered myocardial patch for cardiac repair in a rat infarct model. Tissue Eng Part A 2014; 20: 1325-1335.
13. Zimmermann, W. H., Melnychenko, I., Wasmeier, G., et al. Engineered heart tissue grafts improve systolic and diastolic function in infarcted rat hearts. Nat Med 2006; 12: 452-8.

14. Sekine, H., Shimizu, T., Hobo, K., et al. Endothelial cell coculture within tissue-engineered cardiomyocyte sheets enhances neovascularization and improves cardiac function of ischemic hearts. Circulation 2008; 118: S145-52.
15. Thomson, J. A., Itskovitz-Eldor, J., Shapiro, S. S., et al. Embryonic stem cell lines derived from human blastocysts. Science 1998; 282: 1145-7.
16. Evans, M. J. and Kaufman, M. H. Establishment in culture of pluripotential cells from mouse embryos. Nature 1981; 292: 154-6.
17. Kehat, I., Kenyagin-Karsenti, D., Snir, M., et al. Human embryonic stem cells can differentiate into myocytes with structural and functional properties of cardiomyocytes. J Clin Invest 2001; 108: 407-14.
18. Lian, X., Zhang, J., Azarin, S. M., et al. Directed cardiomyocyte differentiation from human pluripotent stem cells by modulating Wnt/beta-catenin signaling under fully defined conditions. Nat Protoc 2013; 8: 162-175.
19. Yu, J., Vodyanik, M. A., Smuga-Otto, K., et al. Induced pluripotent stem cell lines derived from human somatic cells. Science 2007; 318: 1917-20.
20. Takahashi, K., Tanabe, K., Ohnuki, M., et al. Induction of pluripotent stem cells from adult human fibroblasts by defined factors. Cell 2007; 131: 861-72.
21. Zhang, J., Wilson, G. F., Soerens, A. G., et al. Functional cardiomyocytes derived from human induced pluripotent stem cells. Circ Res 2009; 104: e30-41.
22. Moretti, A., Bellin, M., Welling, A., et al. Patient-Specific Induced Pluripotent Stem-Cell Models for Long-QT Syndrome. New Engl J Med 2010; 363: 1397-1409.
23. Yazawa, M., Hsueh, B., Jia, X. L., et al. Using induced pluripotent stem cells to investigate cardiac phenotypes in Timothy syndrome. Nature 2011; 471: 230-U120.
24. Tulloch, N. L., Muskheli, V., Razumova, M. V., et al. Growth of Engineered Human Myocardium With Mechanical Loading and Vascular Coculture. 2011; 109: 47-59.
25. Wendel, J. S., Ye, L., Tao, R., et al. Functional Effects of a Tissue-Engineered Cardiac Patch From Human Induced Pluripotent Stem Cell-Derived Cardiomyocytes in a Rat Infarct Model. Stem Cells Transl Med 2015; 4: 1324-1332.
26. Banerjee, I., Fuseler, J. W., Price, R. L., et al. Determination of cell types and numbers during cardiac development in the neonatal and adult rat and mouse. Am J Physiol Heart Circ Physiol 2007; 293: H1883-91.
27. Zhang, D., Shadrin, I. Y., Lam, J., et al. Tissue-engineered cardiac patch for advanced functional maturation of human ESC-derived cardiomyocytes. Biomaterials 2013; 34: 5813-5820.
28. Mishra, R., Roux, B. M., Posukonis, M., et al. Effect of prevascularization on in vivo vascularization of poly(propylene fumarate)/fibrin scaffolds. Biomaterials 2016; 77: 255-66.
29. Takebe, T., Koike, N., Sekine, K., et al. Engineering of human hepatic tissue with functional vascular networks. Organogenesis 2014; 10: 260-7.
30. Whisler, J. A., Chen, M. B. and Kamm, R. D. Control of perfusable microvascular network morphology using a multiculture microfluidic system. Tissue Eng Part C Methods 2014; 20: 543-52.

31. Adams, W. J., Zhang, Y., Cloutier, J., et al. Functional vascular endothelium derived from human induced pluripotent stem cells. Stem Cell Reports 2013; 1: 105-13.
32. Aird, A. L., Nevitt, C. D., Christian, K., et al. Adipose-derived stromal vascular fraction cells isolated from old animals exhibit reduced capacity to support the formation of microvascular networks. Exp Gerontol 2015; 63: 18-26.
33. Lin, Y., Weisdorf, D. J., Solovey, A., et al. Origins of circulating endothelial cells and endothelial outgrowth from blood. J Clin Invest 2000; 105: 71-7.
34. Allt, G. and Lawrenson, J. G. Pericytes: cell biology and pathology. Cells Tissues Organs 2001; 169: 1-11.
35. Chang, W. G., Andrejecsk, J. W., Kluger, M. S., et al. Pericytes modulate endothelial sprouting. Cardiovasc Res 2013; 100: 492-500.
36. von Tell, D., Armulik, A. and Betsholtz, C. Pericytes and vascular stability. Exp Cell Res 2006; 312: 623-9.
37. Grainger, S. J. and Putnam, A. J. Assessing the permeability of engineered capillary networks in a 3D culture. PLoS One 2011; 6: e22086.
38. Nakatsu, M. N., Sainson, R. C., Aoto, J. N., et al. Angiogenic sprouting and capillary lumen formation modeled by human umbilical vein endothelial cells (HUVEC) in fibrin gels: the role of fibroblasts and Angiopoietin-1. Microvasc Res 2003; 66: 102-12.
39. Chen, X., Aledia, A. S., Popson, S. A., et al. Rapid anastomosis of endothelial progenitor cell-derived vessels with host vasculature is promoted by a high density of cotransplanted fibroblasts. Tissue Eng Part A 2010; 16: 585-94.
40. Davis, G. E., Kim, D. J., Meng, C. X., et al. Control of vascular tube morphogenesis and maturation in 3D extracellular matrices by endothelial cells and pericytes. Methods Mol Biol 2013; 1066: 17-28.
41. Vapniarsky, N., Arzi, B., Hu, J. C., et al. Concise Review: Human Dermis as an Autologous Source of Stem Cells for Tissue Engineering and Regenerative Medicine. Stem Cells Transl Med 2015; 4: 1187-98.
42. Yeong, W. Y., Sudarmadji, N., Yu, H. Y., et al. Porous polycaprolactone scaffold for cardiac tissue engineering fabricated by selective laser sintering. Acta Biomater 2010; 6: 2028-34.
43. Engelmayr, G. C., Jr., Cheng, M., Bettinger, C. J., et al. Accordion-like honeycombs for tissue engineering of cardiac anisotropy. Nat Mater 2008; 7: 1003-10.
44. Caspi, O., Lesman, A., Basevitch, Y., et al. Tissue Engineering of Vascularized Cardiac Muscle From Human Embryonic Stem Cells. 2007; 100: 263-272.
45. Radisic, M., Euloth, M., Yang, L., et al. High-density seeding of myocyte cells for cardiac tissue engineering. Biotechnol Bioeng 2003; 82: 403-14.
46. Dar, A., Shachar, M., Leor, J., et al. Optimization of cardiac cell seeding and distribution in 3D porous alginate scaffolds. Biotechnol Bioeng 2002; 80: 305-12.
47. Li, R. K., Jia, Z. Q., Weisel, R. D., et al. Survival and function of bioengineered cardiac grafts. Circulation 1999; 100: II63-9.
48. Ifkovits, J. L., Devlin, J. J., Eng, G., et al. Biodegradable fibrous scaffolds with tunable properties formed from photo-cross-linkable poly(glycerol sebacate). ACS Appl Mater Interfaces 2009; 1: 1878-86.

49. Zhang, B., Montgomery, M., Davenport-Huyer, L., et al. Platform technology for scalable assembly of instantaneously functional mosaic tissues. Sci Adv 2015; 1: e1500423.
50. Zimmermann, W. H., Schneiderbanger, K., Schubert, P., et al. Tissue engineering of a differentiated cardiac muscle construct. Circ Res 2002; 90: 223-30.
51. Masumoto, H., Ikuno, T., Takeda, M., et al. Human iPS cell-engineered cardiac tissue sheets with cardiomyocytes and vascular cells for cardiac regeneration. Sci Rep 2014; 4: 6716.
52. Sakaguchi, K., Shimizu, T. and Okano, T. Construction of three-dimensional vascularized cardiac tissue with cell sheet engineering. J Control Release 2015; 205: 83-8.
53. Sekine, H., Shimizu, T., Sakaguchi, K., et al. In vitro fabrication of functional three-dimensional tissues with perfusable blood vessels. Nat Commun 2013; 4: 1399.
54. Amano, Y., Nishiguchi, A., Matsusaki, M., et al. Development of vascularized iPSC derived 3D-cardiomyocyte tissues by filtration Layer-by-Layer technique and their application for pharmaceutical assays. Acta Biomater 2016; 33: 110-21.
55. Matsusaki, M., Kadowaki, K., Nakahara, Y., et al. Fabrication of cellular multilayers with nanometer-sized extracellular matrix films. Angew Chem Int Ed Engl 2007; 46: 4689-92.
56. Nishiguchi, A., Yoshida, H., Matsusaki, M., et al. Rapid construction of three-dimensional multilayered tissues with endothelial tube networks by the cell-accumulation technique. Adv Mater 2011; 23: 3506-10.
57. Mihic, A., Li, J., Miyagi, Y., et al. The effect of cyclic stretch on maturation and 3D tissue formation of human embryonic stem cell-derived cardiomyocytes. Biomaterials 2014; 35: 2798-2808.
58. Hirt, M. N., Boeddinghaus, J., Mitchell, A., et al. Functional improvement and maturation of rat and human engineered heart tissue by chronic electrical stimulation. J Mol Cell Cardiol 2014; 74: 151-161.
59. Chan, Y. C., Ting, S., Lee, Y. K., et al. Electrical stimulation promotes maturation of cardiomyocytes derived from human embryonic stem cells. J Cardiovasc Transl Res 2013; 6: 989-999.
60. Dvir, T., Levy, O., Shachar, M., et al. Activation of the ERK1/2 cascade via pulsatile interstitial fluid flow promotes cardiac tissue assembly. Tissue engineering 2007; 13: 2185-93.
61. Radisic, M., Yang, L., Boublik, J., et al. Medium perfusion enables engineering of compact and contractile cardiac tissue. Am J Physiol Heart Circ Physiol 2004; 286: H507-16.
62. Chan, J. M., Zervantonakis, I. K., Rimchala, T., et al. Engineering of in vitro 3D capillary beds by self-directed angiogenic sprouting. PLoS One 2012; 7: e50582.
63. Moya, M. L., Hsu, Y. H., Lee, A. P., et al. In vitro perfused human capillary networks. Tissue Eng Part C Methods 2013; 19: 730-7.
64. Moya, M. L., Alonzo, L. F. and George, S. C. Microfluidic device to culture 3D in vitro human capillary networks. Methods Mol Biol 2014; 1202: 21-7.

65. Wang, X., Phan, D. T., Sobrino, A., et al. Engineering anastomosis between living capillary networks and endothelial cell-lined microfluidic channels. Lab Chip 2016; 16: 282-90.
66. Lesman, A., Habib, M., Caspi, O., et al. Transplantation of a tissue-engineered human vascularized cardiac muscle. Tissue Eng Part A 2010; 16: 115-25.
67. Schaefer, J. A. and Tranquillo, R. T. Tissue Contraction Force Microscopy for Optimization of Engineered Cardiac Tissue. Tissue Eng Part C Methods 2016; 22: 76-83.
68. Sun, N., Yazawa, M., Liu, J. W., et al. Patient-Specific Induced Pluripotent Stem Cells as a Model for Familial Dilated Cardiomyopathy. Sci Transl Med 2012; 4: 1-13.
69. Barocas, V. H. and Tranquillo, R. T. An anisotropic biphasic theory of tissue-equivalent mechanics: the interplay among cell traction, fibrillar network deformation, fibril alignment, and cell contact guidance. J Biomech Eng 1997; 119: 137-45.
70. Klebe, R. J., Caldwell, H. and Milam, S. Cells Transmit Spatial Information by Orienting Collagen-Fibers. Matrix 1990; 9: 451-458.
71. Munevar, S., Wang, Y. and Dembo, M. Traction force microscopy of migrating normal and H-ras transformed 3T3 fibroblasts. Biophys J 2001; 80: 1744-57.
72. Rodriguez, M. L., Graham, B. T., Pabon, L. M., et al. Measuring the contractile forces of human induced pluripotent stem cell-derived cardiomyocytes with arrays of microposts. J Biomech Eng 2014; 136: 051005.
73. Kim, K., Taylor, R., Sim, J. Y., et al. Calibrated micropost arrays for biomechanical characterisation of cardiomyocytes. Micro Nano Lett 2011; 6: 317-322.
74. Tan, J. L., Tien, J., Pirone, D. M., et al. Cells lying on a bed of microneedles: an approach to isolate mechanical force. Proc Natl Acad Sci U S A 2003; 100: 1484-9.
75. Engler, A. J., Carag-Krieger, C., Johnson, C. P., et al. Embryonic cardiomyocytes beat best on a matrix with heart-like elasticity: scar-like rigidity inhibits beating. J Cell Sci 2008; 121: 3794-802.
76. Jacot, J. G., McCulloch, A. D. and Omens, J. H. Substrate stiffness affects the functional maturation of neonatal rat ventricular myocytes. Biophys J 2008; 95: 3479-87.
77. Bhana, B., Iyer, R. K., Chen, W. L., et al. Influence of substrate stiffness on the phenotype of heart cells. Biotechnol Bioeng 2010; 105: 1148-60.
78. Tibbitt, M. W. and Anseth, K. S. Hydrogels as extracellular matrix mimics for 3D cell culture. Biotechnol Bioeng 2009; 103: 655-63.
79. Boudou, T., Legant, W. R., Mu, A., et al. A microfabricated platform to measure and manipulate the mechanics of engineered cardiac microtissues. Tissue Eng Part A 2012; 18: 910-9.
80. Hinds, S., Bian, W. N., Dennis, R. G., et al. The role of extracellular matrix composition in structure and function of bioengineered skeletal muscle. Biomaterials 2011; 32: 3575-3583.
81. Lee, K.-M., Tsai, K., Wang, N., et al. Extracellular matrix and pulmonary hypertension: control of vascular smooth muscle cell contractility Am J Physiol 1998; 274: H76-82.
82. Moon, A. G. and Tranquillo, R. T. Fibroblast-Populated Collagen Microsphere Assay of Cell Traction Force .1. Continuum Model. Aiche J 1993; 39: 163-177.

83. Legant, W. R., Pathak, A., Yang, M. T., et al. Microfabricated tissue gauges to measure and manipulate forces from 3D microtissues. Proc Natl Acad Sci U S A 2009; 106: 10097-102.
84. Lam, V. and Wakatsuki, T. Hydrogel tissue construct-based high-content compound screening. J Biomol Screen 2011; 16: 120-8.
85. Hansen, A., Eder, A., Bonstrup, M., et al. Development of a drug screening platform based on engineered heart tissue. Circ Res 2010; 107: 35-44.
86. Sbalzarini, I. F. and Koumoutsakos, P. Feature point tracking and trajectory analysis for video imaging in cell biology. J Struct Biol 2005; 151: 182-95.
87. Calve, S. and Simon, H. G. Extracellular Control of Limb Regeneration. K. Garikipati and E. M. Arruda, eds. IUTAM Symposium on Cellular, Molecular and Tissue Mechanics. Springer Netherlands, 2010, pp. 257-266.
88. Noorman, M., van der Heyden, M. A., van Veen, T. A., et al. Cardiac cell-cell junctions in health and disease: Electrical versus mechanical coupling. J Mol Cell Cardiol 2009; 47: 23-31.
89. Menasche, P., Hagege, A. A., Vilquin, J. T., et al. Autologous skeletal myoblast transplantation for severe postinfarction left ventricular dysfunction. J Am Coll Cardiol 2003; 41: 1078-1083.
90. Yu, J., Vodyanik, M. A., Smuga-Otto, K., et al. Induced pluripotent stem cell lines derived from human somatic cells. Science 2007; 318: 1917-1920.
91. Komae, H., Sekine, H., Dobashi, I., et al. Three-dimensional functional human myocardial tissues fabricated from induced pluripotent stem cells. J Tissue Eng Regen Med 2015;
92. Amano, Y., Nishiguchi, A., Matsusaki, M., et al. Development of vascularized iPSC derived 3D-cardiomyocyte tissues by filtration Layer-by-Layer technique and their application for pharmaceutical assays. Acta Biomater 2016; 33: 110-121.
93. Riemenschneider, S. B., Mattia, D. J., Wendel, J. S., et al. Inosculation and perfusion of pre-vascularized tissue patches containing aligned human microvessels after myocardial infarction. Biomaterials 2016; 97: 51-61.
94. Mishra, R., Roux, B. M., Posukonis, M., et al. Effect of prevascularization on in vivo vascularization of poly(propylene fumarate)/fibrin scaffolds. Biomaterials 2016; 77: 255-266.
95. Chen, X., Aledia, A. S., Ghajar, C. M., et al. Prevascularization of a fibrin-based tissue construct accelerates the formation of functional anastomosis with host vasculature. Tissue Eng Part A 2009; 15: 1363-1371.
96. Chen, X., Aledia, A. S., Popson, S. A., et al. Rapid anastomosis of endothelial progenitor cell-derived vessels with host vasculature is promoted by a high density of cotransplanted fibroblasts. Tissue Eng Part A 2010; 16: 585-594.
97. Lin, Y., Weisdorf, D. J., Solovey, A., et al. Origins of circulating endothelial cells and endothelial outgrowth from blood. J Clin Invest 2000; 105: 71-77.
98. Morin, K. T., Smith, A. O., Davis, G. E., et al. Aligned human microvessels formed in 3D fibrin gel by constraint of gel contraction. Microvasc Res 2013; 90: 12-22.

99. Fonck, E., Feigl, G. G., Fasel, J., et al. Effect of aging on elastin functionality in human cerebral arteries. Stroke 2009; 40: 2552-2556.
100. Rezakhaniha, R., Agianniotis, A., Schrauwen, J. T., et al. Experimental investigation of collagen waviness and orientation in the arterial adventitia using confocal laser scanning microscopy. Biomech Model Mechanobiol 2012; 11: 461-473.
101. Bedada, F. B., Chan, S. S., Metzger, S. K., et al. Acquisition of a quantitative, stoichiometrically conserved ratiometric marker of maturation status in stem cell-derived cardiac myocytes. Stem Cell Reports 2014; 3: 594-605.
102. Bhavsar, P. K., Dhoot, G. K., Cumming, D. V., et al. Developmental expression of troponin I isoforms in fetal human heart. FEBS Lett 1991; 292: 5-8.
103. Sasse, S., Brand, N. J., Kyprianou, P., et al. Troponin I gene expression during human cardiac development and in end-stage heart failure. Circ Res 1993; 72: 932-8.
104. Cumming, D. V., Seymour, A. M., Rix, L. K., et al. Troponin I and T protein expression in experimental cardiac hypertrophy. Cardioscience 1995; 6: 65-70.
105. Zhao, Y. Y., Sawyer, D. R., Baliga, R. R., et al. Neuregulins promote survival and growth of cardiac myocytes. Persistence of ErbB2 and ErbB4 expression in neonatal and adult ventricular myocytes. J Biol Chem 1998; 273: 10261-10269.
106. Hsieh, P. C., Davis, M. E., Gannon, J., et al. Controlled delivery of PDGF-BB for myocardial protection using injectable self-assembling peptide nanofibers. J Clin Invest 2006; 116: 237-248.
107. Siedner, S., Kruger, M., Schroeter, M., et al. Developmental changes in contractility and sarcomeric proteins from the early embryonic to the adult stage in the mouse heart. J Physiol 2003; 548: 493-505.
108. Garcia, N. A., Ontoria-Oviedo, I., Gonzalez-King, H., et al. Glucose Starvation in Cardiomyocytes Enhances Exosome Secretion and Promotes Angiogenesis in Endothelial Cells. PLoS One 2015; 10: e0138849.
109. Banai, S., Shweiki, D., Pinson, A., et al. Upregulation of vascular endothelial growth factor expression induced by myocardial ischaemia: implications for coronary angiogenesis. Cardiovasc Res 1994; 28: 1176-9.
110. Dickinson, R. B., Guido, S. and Tranquillo, R. T. Biased cell migration of fibroblasts exhibiting contact guidance in oriented collagen gels. Ann Biomed Eng 1994; 22: 342-356.
111. Laco, F., Grant, M. H. and Black, R. A. Collagen-nanofiber hydrogel composites promote contact guidance of human lymphatic microvascular endothelial cells and directed capillary tube formation. J Biomed Mater Res A 2013; 101: 1787-1799.
112. Morin, K. T. and Tranquillo, R. T. Guided sprouting from endothelial spheroids in fibrin gels aligned by magnetic fields and cell-induced gel compaction. Biomaterials 2011; 32: 6111-6118.
113. Hernandez Vera, R., Genove, E., Alvarez, L., et al. Interstitial fluid flow intensity modulates endothelial sprouting in restricted Src-activated cell clusters during capillary morphogenesis. Tissue Eng Part A 2009; 15: 175-185.